Escola Politécnica - USP

Engenharia Elétrica – Sistemas Eletrónicos

Trabalho de Formatura

A COMSOL Multiphysics model for CV test on ruthenium/TPrA ECL system.

Orientador:
Fernando J. Fonseca
Colaboradores:
Danilo Demarchi
Alessandro Sanginario
Gerson Santos

Candidato:
Rodrigo S. Pereira
6485893

Ano Acadêmico: 2013

Resumo extendido

Neste trabalho, um modelo em COMSOL Multiphysics para o teste de voltametria cíclica sobre a luminescência eletroquímica do sistema baseado em rutênio usando a amina TPrA como correagente é proposto. O modelo considera apenas a reação principal so sistema e se baseia em uma aproximação unidimensional da célula eletroquímica. Diversos fenômenos, como a influência do pH sobre a intensidade do sinal luminoso, foram ignorados já que o objetivo do modelo é oferecer uma primeira aproximação do fenômeno.

Voltametria cíclica é uma técnica útil e versátil para o estudo de substâncias eletronicamente ativas. Este teste constitui na medição da corrente, limitada pela difusão dos portadores de carga na interface entre o eletrodo e o eletrólito, na célula eletroquímica gerada pela aplicação de uma excitação triangular de potencial elétrico. Esse tipo de teste é muito popular na caracterização de eletrodos devido aos diversos parâmetros que podem ser extraidos de seu resultado. Detalhes sobre esta técnica de voltametria, bem como uma breve introdução à eletroquímica, estão presente no capítulo 1 deste trabalho.

Luminescência eletroquímica (ECL) é a produção de luz através de um processo eletroquímico. Como os demais fenomenos de luminescência, não há produção ou consumo de calor assossiado à emissão de luz. Inicialmente, as técnicas de ECL se baseavam em aniquilação iônica, que envolve a formação de ânios e cátions na célula eletroquímica. Quando se encontram, esses íons trocam elétrons e regeneram a especie inicial, mas com elétrons em estado excitado. A energia liberada pelo decaimento destes elétrons é em forma de luz, daí o fenômeno da luminescência. Geralmente, a mesma substância forma os ânions e cátions para este tipo de sistema, mas isso não é obrigatorio.

Atualmente, os sistemas de ECL empregam coreagentes, substâncias químicas que não produzem elétrons em estados exitados, mas que ao reagirem com a substância luminogenera, induzem a formação de átomos em estado excitado. Neste tipo de sistema, ambas as substâncias são oxidadas ou reduzidas, o que simplifica o projeto dos eletrodos utilizados na célula eletroquímica. O coreagente oxidado/reduzido se torna uma substância reativa que interagem com a forma oxidada ou reduzida da substância luminogenera. A reação produz o estado exitado e o sistema emite luz enquanto regenera a substância luminogenera e consome o correagente.

O uso de sistemas de ECL baseados em correagentes prevaleceu sobre os sistemas baseados em aniquilação iônica porque aumentou o número de substâncias que apresentam o fenômeno de ECL, oferece sistemas com melhor rendimento e foi a única maneira encontrada de se obter ECL em meios aquosos.

Explicações detalhadas sobre ECL baseada em aniquilação iônica e correagentes se encontra no capítulo 2.

Dentre os diversos sistemas de ECL baseados em correagentes, o par $Ru(bpy)_2^{3+}$/TPrA está à sua elevada eficiência e aplicações em testes imunologicos e de detecção de DNA. TPrA é uma abreviatura para tri-n-propylamina. A descrição detalhada deste sistema, que é o utilizado no modelo deste trabalho, está no capítulo 3.

ECL possui varias aplicações interessantes no campo biomédico atuando como sensor. A habilidade do rutênio de formar sistemas luminescentes na presença de aminas o torna uma substância interessante na detecção de DNA, por exemplo, já que este forma um sistema luminescente com a Guanina (base nitrogenada constituinte do DNA). Tais sistemas apresentam elevada sensibilidade, sendo úteis para detectar descasamento de bases ou pequenas concentrações de DNA.

Também é possivel marcar a susbtância que se deseja detectar com o grupo do rutênio, assim, na presença do coreagente e da aplicação do potencial elétrico adequado, a presença da substância será detectada.

Sensores baseados em ECL são interessantes por oferecerem uma sensibilidade elevada e por serem de leitura extremamente simples, já que a saida do sistema é um sinal luminoso caso a substância que se deseja detectar esteja presente na solução.

O capítulo 4 deste trabalho trás alguns exemplos de aplicação para ECL bem como os materiais que são utilizados atualmente para a fabricação de microeletrodos que visam esse tipo de sistema.

O modelo foi construido no software COMSOL Multiphysics, versão 4.3b. COMSOL é um software de elementos finitos com um banco de equações diferenciais provenientes de diversas áreas de engenharia e ciências. Para este trabalho, o modulo utilizado foi o de eletroquímica. Detalhes sobre as equações envolvidas no modelo se encontram no capítulo 5 deste trabalho.

Os resultados oferecidos pelo modelo estão na forma de gráficos, presentes no na seção "Results" do capítulo 5. Esses gráficos mostram como o sistema simulado deveria se comportar, em termos de corrente, tensão, concentração das substancias químicas e sinal luminoso. Felizmente, os resultados apresentados pelo modelo são coerentes com aqueles observados nos experimentos realizados no laboratório MiNES, do Politecnico di Torino.

As reações secundárias do sistema de luminescência foram adicionadas ao modelo durante o período de estudos remanescente na Escola Politécnica. Essas modificações alteraram substancialmente as predições do modelo. Infelizmente, os novos resultados não puderam ser comparados com dados experimentais, já que eles eram provenientes do laboratório do Politecnico di Torino.

O modelo foi idealizado para apoiar os estudos sobre ECL que vem sendo realizados no Politecnico di Torino e estabelecer um ponto de partida para modelos mais detalhados em fenomenos envolvendo ECL. Ao fim do trabalho, obteve-se um modelo de simples aplicação e que

pode ser facilmente modificado para se observar como diferentes concentrações e/ou potenciais irão alterar o comportamento do sistema.

O fenômeno de ECL tem larga aplicabilidade no cenário nacional, podendo ser utilizado para a fabricação de sensores capazes de detectar concentrações extremamente baixas de moleculas biologicas, a depender da técnica utilizada para fixar o grupo luminescente à substância desejada. Tal detecção é importante para, por exemplo, testes de contaminação ou deterioração em alimentos, tal como o leite. A fácil leitura de tais sensores os tornam atraentes, pois não é necessaria uma pessoa com conhecimento técnico para estabelecer se a amostra está ou não contaminada. Também, ECL é uma técnica superior a outras luminescências em termos de produção de sensores porque o usuário tem total controle sobre o fenômeno, pois este depende da aplicação de um potencial elétrico para ocorrer.

Motivação

A motivação deste trabalho de conclusão de curso foi fornecer um modelo para o sistema de ECL $Ru(bpy)_2^{3+}$/TprA que servisse de apoio aos experimentos realizados no MiNES, laboratório do Politecnico di Torino. O modelo tem o objetivo de oferecer uma resposta qualitativa do sistema, diminuindo assim a quantidade de experimentos que devem ser realizados para caracterisar adequadamente os limites deste sistema de ECL.

ECL já é um fenômeno bem estudado pela comunidade científica e possui diversas aplicações práticas, a principal delas sendo o projeto do sensores, que – dadas as características do fenômeno – são de fácil leitura. Os campos que mais utilizam ECL são testes imunológicos, detecção de DNA e RNA, detecção de açucares e detecção de proteínas.

Atualmente, os estudos acadêmicos realizados em ECL podem ser resumidos em dois grandes grupos: A busca de maneiras para tornar uma determinada substância detectável atráves de um sistema de ECL; a busca de materiais e formatos para microeletrodos que melhorem o rendimento e a eficiência do sistema de ECL. Assim tornando a ECL um fenômeno de caráter interdisciplinar, interessante para químicos, engenheiros de materiais, engenheiros eletrônicos.

O presente trabalho trás as principais aplicações de ECL descritos com algum detalhe no capítulo 4. A citar, as aplicações mais interessantes do ponto de vista da eletrônica são:

- Filmes finos para ECL, pág. 35;
- Materiais nanométricos utilizados em sensores baseados em ECL, pág. 40.

O modelo apresentado neste trabalho tem foco na caracterização do microeletrodo utilizado, tendo como principais preocupações a produção de uma estimativa razoável para a corrente que flui através do eletrolíto e a estimativa qual

Summary

In this work, a COMSOL Multiphysics model for the ruthenium/TPrA ElectroChemiLuminescence (ECL) cyclic voltammery test is proposed. The model considers only the first reaction wave of the system and is based on an one dimension geometry. Several phenomenons, such as the pH influence in the ECL signal intensity, were ignored in order to provide a model that does not demands to much computational power and can be used in personal computers.

Cyclic voltammetry tests are an useful and versatile technique for studying electro-active species. It constitutes on the measuring the current, limited by the diffusion of the charge carriers at the electrode/electrolyte interface, generated by a periodic triangular wave as potential stimulus. These tests are very popular on the characterization of electrodes because of the many parameters that can be extracted from it.

The $Ru(bpy)_3^{2+}/TPrA$ is one of the most popular ECL coreactant systems because its applications on immunoassays and DNA probe assays. TPrA standing for Tri-n-propylamine.

The model was build in a way that modifications can be easily implemented, making it useful for simulating experimental tests with this specific ECL system, providing, in a quick way, the general behavior of the system. Also, because the way that it was build, the model can be quickly modified to simulate other ECL systems.

Version 4.3b of COMSOL Multiphysics was utilized in this work because it is the first one when the software offers a specific module for electroanalysis studies, and this update has largely improved the electrochemical branch of physics, as well its documentation.

The model was idealized to help the ECL studies that are performed on Politecnico di Torino and to establish a starting point for future ECL phenomenons modeling.

The last part of the work is a complement to the model where the side reactions are implemented. This update has changeg significantly the overall

behavior of the system, introducing a transient and forcing the application of 15 voltametric cycles to proper characterize the system.77

List of Figures

List of Tables

Contents

Chapter 1

Introduction

Electrochemistry is the branch is chemistry that studies the relation between electrical and chemical phenomena. Usually, the solution takes or provide electric energy to the external system.

A considerable part of these studies are concerned about the effects of a current passing through an ionic solution or the production of electric energy by chemical reactions. This is a very large field of study, it covers a large variety of phenomenas, like corrosion, devices, like batteries, and techniques, like metal deposition or aluminum mass production. The basic principles presented in this chapter are present in every single electrochemical phenomena. However, this work is concern about the light emission by electrochemical reactions, called electrochemiluminescence (ECL).

1.1 Electrochemical Cells

Electrochemical cell are composed by electrodes and an electrolyte. An electrode is made by an electronic conductor, it can be made of solid or liquid metal (Pt, Au, Hg), carbon or semiconductors. The electrolyte is a solution where electric charge is carried ions. Liquid solutions are the most common type of electrolyte, they contain ionic species like H^+, Na^+, Cl^-. The solvent is often water, but this is not mandatory. In order to transport charge, the electrolyte must have a sufficient conductive, so it is possible to use supportive salts to enhance the conductivity of the solution.

In general, electorchemistry deals with situations where oxidation and reduction reactions are separated in space or time, connected by an external

electric circuit.

Reduction-oxidation (redox) reactions are chemical reactions in which atoms have their oxidation state changed. This means that these reactions involve the transfer of electrons between species. If a specie gain an electron, is said that the specie is reducted, so we have a reduction reaction. If a specie lose an electron, is said that the specie is oxidize, so we have an oxidation reaction.

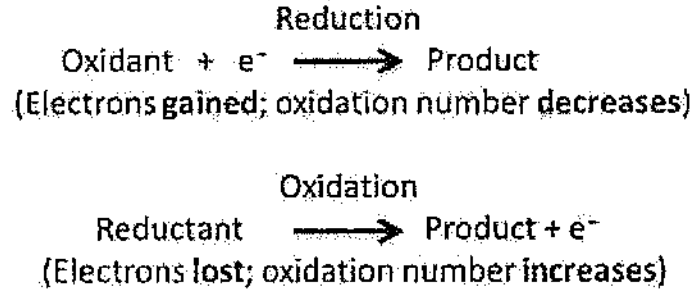

Figure 1.1: Redox reactions

Redox reactions have many similarities with acid-base reactions. Like acid-base reactions, redox reactions are a matched set, that is, there cannot be an oxidation reaction without a reduction reaction happening simultaneously. The oxidation or reduction reactions alone are called half-reaction. In electrochemical cells, one half-reaction occurs in the electrode and the other in the electrolyte. In order to begin the reaction, the system must overcome an energy barrier. This barrier is called oxidation or reduction potential and it is measured in volts. If the oxidation potential is positive, it means that the system must provide energy to the pair electrode/electrolyte in order to force the reaction to happen. An example of non spontaneous reaction is the production of aluminum, where a great amount of electric energy must be used in order to force the deposition of aluminum. In the same way, if the potential is negative, the reaction is spontaneous. An example is the oxidation of iron in bicycles left in open air for too long. The oxidation and reduction potentials are symmetric, if a species has an oxidation potential of E, its reduction potential will be $-E$.

Considering this, controlling the potential applied into an electrochemical cell is essential for studies and experiments in electrochemistry. It can be measured between the two electrodes of the cell and it represents the avail-

able energy that drives the charges externally between the electrodes.

Before continue with further explanations,it is important to explain the notation that is used to represent electrochemical cell structures. The cell represented on Figure 1.2 can be represented as:

$$Zn/Zn^{2+},Cu^{2+}/Cu \tag{1.1}$$

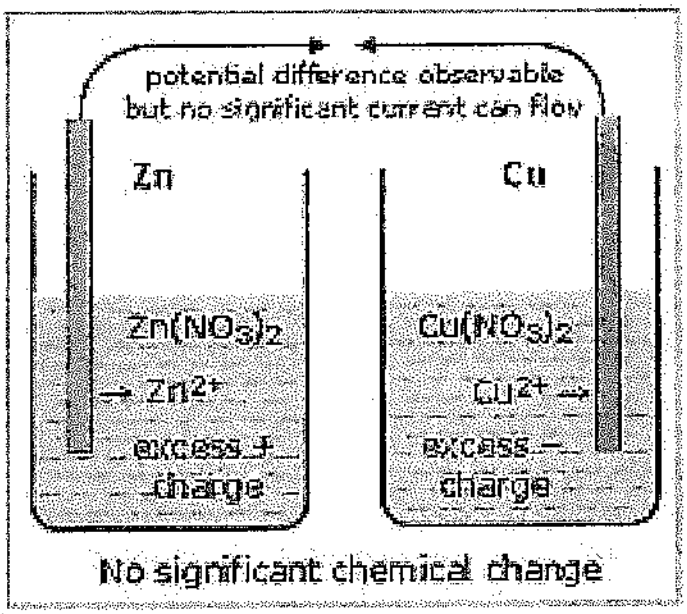

Figure 1.2: Electrochemical cell

This is the compact notation for electrochemical cells. The slash represents the phase boundary, the comma separates the components of the same phase. A double slash, not present in this example, represents a phase boundary whose potential is considered to be a negligible component of the overall cell potential. The overall chemical reaction taking place in a cell is made up of two independent half-reactions, which describe the chemical changes at the two electrodes. In the example case, one half reaction is the zinc oxidation. The zinc atoms in the electro lose electrons an jump to the solution, consuming the electrode material. The other half reaction is the copper reduction. The copper atoms in the solution gain electrons and are deposited in the electrode. It is an example of non spontaneous electrochemical cell. Each half reaction responds to the interface potential difference at the corresponding

electrode. Most of the time, only one of these half-reactions is of interest. So, the electrode at which it occurs is called working electrode. To focus on it, the other half of the electrochemical cell is standardized by using a reference electrode, made up of phases having, essentially, constant composition. The internationally accepted reference is the standard hydrogen electrode (SHE), also called normal hydrogen electrode (NHE) which has all components at a unit activity:

$$Pt/H_2/H^2 \tag{1.2}$$

Potentials are often measured and quoted with respect to reference electrodes different from the NHE. Two of the most popular are the saturated calomel electrode (SCE), with a potential of 0.242 V vs. NHE, and the silver-silver chloride electrode (usually represented in literature as "vs. Ag/AgCl"), with a potential of 0.197 V vs. NHE.

$$Hg/Hg_2Cl_2/KCl(SCE) \tag{1.3}$$

$$Ag/AgCl/KCl(us.AgCl) \tag{1.4}$$

Since the reference electrode has a constant composition, its potential is fixed. Hence, any changes in the cell are caused by the working electrode. We say that we observe or control the working electrodes potential with respect to the reference electrode. Driving the working electrode to negative potentials, the electrons energy is raised. Eventually, they can reach a high enough level to transfer into a vacant electronic state on species from the electrolyte. When this happens, the electrons flow from the electrode to the electrolyte is called reduction current. On the same working principle, when the electrode potential is positive, the electrons of species from the electrolyte will find a state of lower energy in the electrode and a current from the electrolyte to the electrode will be formed, called oxidation current. The critical potentials at which these processes occurs are related from the standard potentials (E^0) for the specific chemical specie. In a solution, the equilibrium concentrations of the reduced and oxidized forms of a redox couple are linked to the potential (E) by the Nernst's equation(Equation1.5).

$$E = E^0 - \frac{RT}{nF} \ln \frac{C_{ox}}{C_{red}} \tag{1.5}$$

Where E^2 is the standard potential, F is the Faraday's constant, T is the absolute temperature, C_{ox} and C_{red} are the concentrations of oxidation and

reduction centers. Electrochemical processes can be studies and understood by using voltammetry, polarography, chronopotentiometry, cyclic voltammetry (CV) and others tests.

1.2 Luminescence

Luminescence is light emission by substances at a low temperature. In luminescence, some energy source moves an electron of an atom out of its normal energy level into a higher energy state (excited state). Then, the electron jumps back to its normal state returning the energy in the form of photons. Normally, the excitation energy is greater than the energy, observed on the light wavelength, emitted. There are several types of luminescence, named according to the energy source that triggers the light emission. In this section, we will expose some examples, such as:

1. Fluorescence and Photoluminescence are luminescences where the energy is provided by electromagnetic radiation, such as light. The difference between these two is that fluorescence is caused by ultraviolet radiation, while photoluminescence can be triggered by any form of electromagnetic radiation.

2. Radio-luminescence is caused by nuclear radiation. Older glow-in-the-dark clock dials often used a paint with a radioactive material and a radio-luminescent material.

3. Chemiluminescence is a luminescence where the energy is provided by a chemical reaction. Examples of chemiluminescence are bio-luminescence, where these reactions occurs inside living form (the most famous example are fireflies) and ECL, where the luminescent reaction is triggered by the oxidation or reduction of the species inside the solution.

Table 1.1 summarizes the most important types of luminescence.

Table 1.1: Different types of luminescence

Luminescence type	caused by
Photoluminescence (PL)	Photo-excitation of compounds
Chemiluminescence (CL)	Chemical excitation of compounds
Electrochemiluminescence (ECL)	Electrogenerated chemical excitation
Radiochemiluminescence	Radiation-induced chemical excitation
Lyoluminescence	Excitation induced by dissolution of an irradiated or other energy-donating solid
Sonoluminescence	Excitation of compounds by ultrasonication, either by energy transfer from the intrinsic SL centers of water or by chemical excitation by hydroxyl radicals and atomic hydrogen

1.3 Voltammetric methods

Voltammetry is a category of electroanalytical methods used in analytical chemistry and many industrial processes. Voltammetry experiments investigate the half cell reactivity of an electrolyte, it is the measurement of the current resulting from the application of a potential, normally utilizing a three-electrode configuration for the electrochemical cell (Figure 1.3). The use of three electrodes (working, auxiliary and reference) along with the potentiostat instrument allows accurate applications of potential functions and measurements of the resulting current. The different voltammetric techniques are distinguished from each other, primarily, by the applied potential function at the working electrode that it utilizes.Voltammetric techniques are divided into subclasses based on the different modes of applying the potential in the electrode. In this work, we will only briefly explain the cyclic voltammetry, that is the technique that will be modeled.

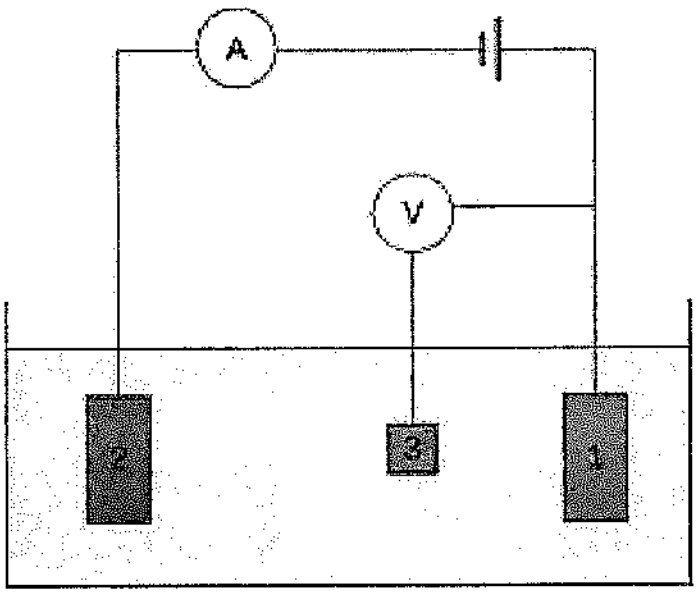

Figure 1.3: Three electrode setup

1.3.1 Cyclic Voltammetry (CV)

CV is an useful and versatile technique for studying electro-active species. It constitutes on the measuring the current, limited by the diffusion of the

charge carriers at the electrode/electrolyte interface, generated by a periodic triangular wave as potential stimulus.

Figure 1.4 illustrate the expected response of a reversible redox couple during a single potential cycle. The test begins with only the oxidized specie (O) present on the electrolyte. So, the scan starts in a negative potential, in a value where no reduction occurs, and is risen according to the scan rate. As the applied potential approaches the characteristic E^0, an equilibrium potential between the electrode and the electrolyte given by the Nernst equation, for the redox process, an increasing cathodic current begins to be measured, and it, eventually reaches a peak. After, the potential reaches the peak of the triangular wave and starts to decrease, the potential peak must be chosen carefully in order to reduct all the present specie O. During the potential decrease, reduced molecules (R) are oxidized back to O, resulting in an anodic current, that have a symmetric behavior to the previous cathodic current. The characteristic peaks on the cyclic voltammogram are caused by the formation of a diffusion layer near the electrode surface. These can be best understood by carefully examining the concentration-distance profiles during the potential sweep.

Figure 1.5 illustrates the concentration gradients of the reactant and product at different times, the first corresponds to the initial potential of the sweep (a), the formal potential of the couple during the forward (b) and reverse scan (d), and the achievement of a zero-reactant surface concentration (c). Observe that the continuous change in the surface concentration is associated with an expansion of the diffusion layer thickness. The resulting current peaks reflect the continuous variation of concentration gradient with respect to time. Hence, the increase in the peak current corresponds to the achievement of diffusion control. It is important to remember that when the overall reaction is controlled just by the rate at which the electro-active species reach the surface, the current is said to be mass-transport-limited, it means that the current is limited by the diffusion of the charge carriers in the electrolyte. Such reactions are called nernstian or reversible.

The most relevant parameters that can be extracted from CV tests are the magnitude of the current peak (I_p), potential peak (E_p), number of transfered electrons per reactant molecule (n), rate constant, diffusion coefficient (D) and electrochemical reversibility. The current peak for a reversible system is described by the Randles-Sevcik equation (Equation 1.6):

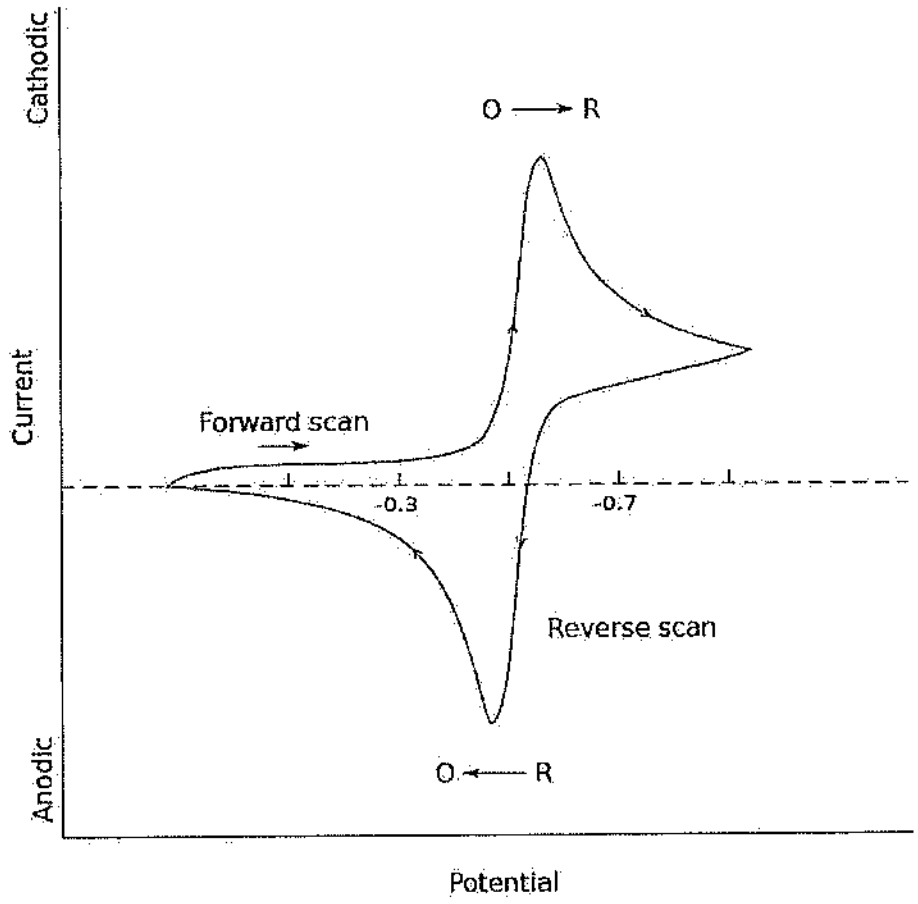

Figure 1.4: Typicall CV graphic

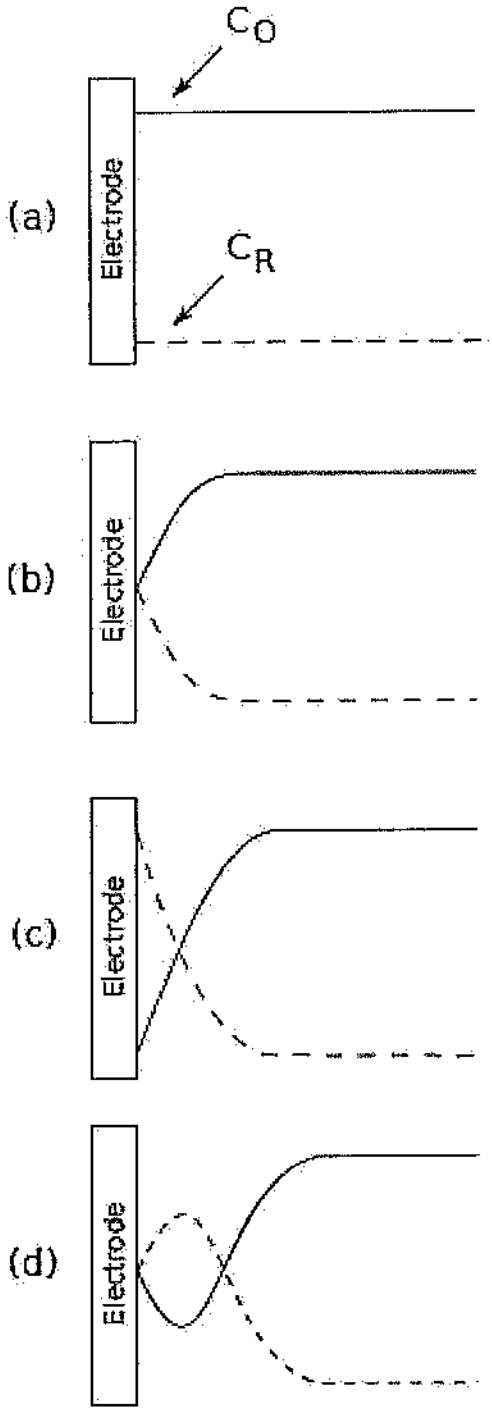

Figure 1.5: Diffusion layer schematic.

$$I_p = (2.69 \times 10^5) \times A \times n^3/2 \times sqrtD \times \nu \times C \tag{1.6}$$

Where A is the active area (cm^2) of the working electrode, n is the number electrons exchanged during the redox process, D (cm^2/s) and C (mol/cm^3) the diffusion coefficient and the electrolyte concentration of the electro-active specie, ν is the scan rate (V/s).
The position of the peaks on the potential axis (E_p) are related to the formal potential of the redox process. The formal potential for a reversible couple is between the anodic peak current potential ($E_{p,a}$) and the cathodic peak current potential ($E_{p,c}$):

$$E^0 = \frac{E_{pa} + E_{pc}}{2} \tag{1.7}$$

The separation between the potential peaks is given by:

$$\Delta E = E_p, a + E_p, c = \frac{0.059}{n} \tag{1.8}$$

These parameters extracted cyclic voltammograms make CV a very useful tool to characterize redox reactions at electrodes. Also, CV is the most popular electrochemical technique for solid electrodes. The production of reproducible results, at least for subsequent cycles, is most valuable for characterizing not well defined electrode surfaces. Also, on CV graphics is possible to observe the oxidation and reduction peaks simultaneously, fact that is helpful while investigating electrode processes.

Chapter 2

ECL

2.1 Historic Background

Electro-chemiluminescence (ECL) is the light generation through electrochemical processes. Normally, the emission is due to the annihilation between a radical anion and cation. This phenomena was first observed in the 1920s when Gringnard compounds were oxidized at several hundred volts[1], and again when luminol was oxidized in an alkaline solution[2]. In 1964, it was shown by Hercules that a square wave potential pulse could be used to generate light in anaerobic medias[3].

After these early experiments, several developments have occurred on ECL, including the use of coreactants that allowed ECL in aqueous solutions[4]. The low detection limit of ECL has made it an useful analysis tool. It is popular on bioanalysis, where it has been applied on enzyme detection, immunosensors and DNA probes. Even if most ECL applications are on biological fields, ECL is also used on studies of organic compounds on anaerobic medias. A time line of ECL development is present on Figure 2.1.

2.2 Ion Annihilation ECL

Even though modern ECL techniques are most often based on the use of a coreactant - which will be exposed on the next sections, the first ECL studies were based on ion annihilation ECL. Ion annihilation ECL involves the formation of an ion with electrons on the excited state as a result of an exergonic electron transfer between electrochemically generated species, often radical ions, at the surface of an electrode.

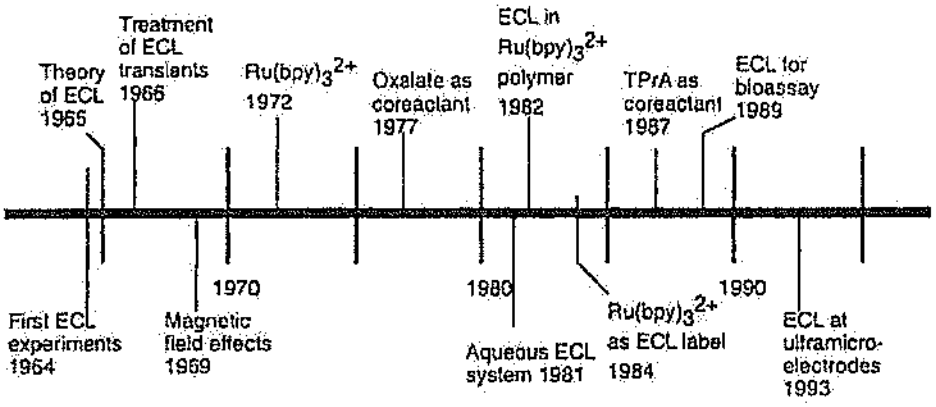

Figure 2.1: ECL time line

$$A - e^- \longrightarrow A^{\cdot+} \tag{2.1}$$

$$A + e^- \longrightarrow A^{\cdot-} \tag{2.2}$$

$$A^{\bullet+} + A^{\bullet+} \longrightarrow A + A^* \tag{2.3}$$

$$A^* \longrightarrow A + h\upsilon \tag{2.4}$$

As shown on equations 2.1 to 2.4, after the emitter specie (A) is oxidized ,equation 2.1 and reduced 2.2, the resulting radical cation ($A+$) and anion (A^-) are annihilated, forming the excited state species (A^*), Equation 2.3, that emits light on its decay, Equation 2.4. Annihilation reactions can also happen in "mixed systems", where the radical cation and radical anion comes from different molecules. Depending on the energy available in the ion annihilation, the produced A can be either the lowest excited singlet state species (^{1}A) or the triplet state species (^{3}A). The enthalpy, which is related to the available energy on the system, can be calculated from the redox potentials of the Equations 2.1 and 2.2 as defined in the Equation 2.5.

$$-\Delta H_{ann} = E_p(R/R^{\bullet+}) - E_p(R^{\bullet-}) - 0.16 \tag{2.5}$$

Where $-\Delta H_{ann}$ (eV) is the enthalpy for ion annihilation, E_p is the potential peak for electrochemical oxidation or reduction (given in Volts), and 0.16 is an approximation for the entropy term ($T\Delta S$) at 25^0C (0.10 eV)

with an addition of 0.057 eV resulting from the difference between the reversible potential and the peak potential of the redox reactions [5]. If the estimated enthalpy ($-\Delta H_{ann}$) from the Equation 2.5 is larger than the energy (Es) required to produce the lowest excited singlet state from the ground state, ^{1}A is directly generated on the system, and the system is called the energy-sufficient and the reaction is said to follow the S-route. A typical example of the energy-sufficient system is the $DPA^{\bullet+}/DPA^{\bullet-}$ (DPA = 9,10-diphenylanthracene) system [6] [7].

$$S-route: A^{\bullet+} + A^{\bullet-} \longrightarrow A + {}^1A^* \tag{2.6}$$

On the other hand, if $-\Delta H_{ann}$ is smaller than E_s but larger than the triplet state energy E_t, ^{3}A is initially formed, and then ^{1}A can be formed by the triplet-triplet annihilation (TTA) as shown in Equation 2.8. This is type so systems are called energy-deficient, and the reaction is said to follow the T-route.$TMPD^{\bullet+}/DPA^{\bullet-}$ and $TMPD^{\bullet-}/AN$ ($TMPD = N,N,N',N'-$tetramethyl-p-pheuylenediamine and AN = anthracene) systems [7] [8] are two examples of energy-deficient systems. In a solution phase, the efficiency of direct emission from ^{3}A is believed to be low because of the long radioactive lifetime of ^{3}A and its quenching by radical ions or other species, like molecular oxygen.

$$T-route: A^{\bullet+} + A^{\bullet-} \longrightarrow A + {}^3A^* \tag{2.7}$$

$${}^3A^* + {}^3A^* \longrightarrow A + {}^1A^* \tag{2.8}$$

If $-\Delta H_{ann}$ is nearly marginal to (Es), the T-route can contribute to the formation of ^{1}A in addition to the S-route; So, the type of system is called the ST-route. A typical example of this kind of system is the rubrene anion-cation annihilation [9], which has been finally confirmed by means of combined magnetic field/temperature and solvent/temperature investigations. In addition to the formation of singlet and triplet excited states, ion annihilation reactions can lead to the direct formation of excimers (excited dimers) and exciplexes (excited complexes). In most cases, the participating molecules must be able to align so that there is significant π-orbital overlap; thus this occurs mostly among planar polycyclic aromatic hydrocarbons (PAHs) such as pyrene and perylene [10]. Other reactions such as TTA process can also lead to the formation of excimers and/or exciplexes [11]. The reactions associated with the formation of excimers and exciplexes are said to follow the E-route. The relevant reactions are summarized in the Equations

2.9, 2.10 and 2.11.

$$A^{\bullet+} + A^{\bullet-} \longrightarrow A_2^* \tag{2.9}$$

$$A^{\bullet+} + A'^{\bullet-} \longrightarrow (AA')^* \tag{2.10}$$

$${}^3A^* + {}^3A^* \longrightarrow {}^1A_2^* \tag{2.11}$$

Excimer or exciplex emission is generally characterized by broad featureless emission red-shifted from the singlet emission of the molecule. Also, the emission wavelength and intensity change with solvent polarity. Emission from the monomer and the excimer are very often observed in the same spectrum [12]. Although excimers and exciplexes can be formed via photoexcitation as observed in fluorescence spectroscopy, they are most likely to form in ECL due to the close proximity of the radical ions in the contact radical ion pair [13]. Moreover, as demonstrated in recent studies [14], the radical ion annihilation pathway of ECL can generate emitting states different from those formed following photoexcitation, and the chemical environment (e.g., medium permissibility, ionic concentration, concentration of reagents) can be adjusted or chosen so as to tune the reaction rates and equilibrium; these effects are manifested in the emission energy and the overall ECL efficiency. For visible range emissions (400-700 nm), (E_s) covers from 3.1 to 1.8 eV, according to the Equation 2.12.

$$E_s = h\upsilon = \frac{hc}{\lambda} \tag{2.12}$$

This means, to produce annihilation ECL, the potential window of an electrochemical system must be wide enough (from, approximately, 3.3 to 2 V, Equation 2.5) so that sufficiently stable radical anions and cations can be generated. As a result, nonaqueous media, such as acetonitrile with tetra-n-butylammonium perchlorate (TBAP) as the supporting electrolyte, are extensively used in the study of ion annihilation ECL. As will be discussed below, the first aqueous ECL system, which was coreactant ECL based, was not reported until 1981 by Rubinstein and Bard [15]. Certain conditions need to be met for the efficient generation of ion annihilation ECL, which include:

1. stable radical ions of the precursor molecules in the electrolyte of interest, which can be evaluated via the cyclic voltammetric (CV) response;

2. good PL efficiency of a product of the electron transfer reaction, which often can be evaluated from the fluorescent experiment;

3. sufficient energy in the electron transfer reaction to produce the excited state as described above.

2.3 Coreactant ECL

Nowadays, all commercially available ECL analytical instruments are based on coreactant ECL technology.Unlike ion annihilation ECL, in which electrolytic generation of both the oxidized and reduced ECL precursors are required, coreactant ECL is generated with a single potential step or one directional potential scanning at an electrode in a solution containing the luminophore, light emitting agent, species in the presence of a deliberately added reagent (coreactant). Depending on the polarity of the applied potential, both the luminophore and the coreactant species can be first oxidized or reduced at the electrode to form radicals, and intermediates formed from the coreactant then decompose to produce a powerful reducing or oxidizing species that reacts with the oxidized or reduced luminophore to produce the excited states that will emit light. Since highly reducing intermediate species are generated after an electrochemical oxidation of a coreactant, or highly oxidizing ones are produced after an electrochemical reduction, the corresponding ECL reactions are often referred to as oxidative-reduction ECL and reductive-oxidation ECL, respectively [19, 25]. Thus, a coreactant is a species that, upon electrochemical oxidation or reduction, immediately undergoes chemical decomposition to form a strong reducing or oxidizing intermediate that can react with an oxidized or reduced ECL luminophore to generate excited states. Use of a coreactant is useful especially when one of $R^{\bullet+}$ or $R^{\bullet-}$ is not stable enough for ECL reaction or when the ECL solvent has a narrow potential window so that $R^{\bullet+}$ or $R^{\bullet-}$ cannot be formed. Additionally, the use of a coreactant can make ECL possible even for some fluorescent compounds that have only a reversible electrochemical reduction or oxidation. When the annihilation reaction between oxidized and reduced species is not efficient, the use of a coreactant may produce a more intense ECL. Finally, the oxygen quenching effect, which is often encountered in ion annihilation ECL, may be eliminated in oxidative-reduction type ECL, so that ECL analysis can be carried out in the air. Note that, as indicated in Equation 2.2 above and discussed in the following sections, in ion annihilation ECL, all starting species (A) can be regenerated after light emission, whereas in a coreactant ECL system, such

Type of coreactant ECL	Coreactant	Main coreactant intermediate	E^0 (V vs NHE)	Refs
oxidative-reductive	oxalate	$CO_2^{\bullet-}$ $CH_3CO^{\bullet}$	$CO_2/CO_2^{\bullet-}$ -1.9V	[54, 55]
	pyruvate/Ce(III)			
	tri-n-propylamine (TPrA)	$TPrA^{\bullet+}, TPrA^{\bullet}$	$TPrA\bullet+/TPrA$ +1.1V	[54][45]
reductive-oxidation	hydrazine (N_2H_4)	$N_2H_2, N_2H_3^{\bullet}$	N_2H_2/N_2 < $-2.3V$	[56, 57]
	persulfate ($S_2O_8^{2-}$)	$SO_4^{\bullet-}$	$SO_4^{\bullet-}/SO_4^{2-}$ +2.9V	[58]
	hydrogen peroxide	$OH^{\bullet}$	$OH^{\bullet}/OH^{-}$ 1.77 to 1.91V	[60]

Table 2.1: Typical coreactant ECL systems for $Ru(bpy)_3^{2+}$ luminophore

as $Ru(bpy)_3^{2+} + Ru(bpy)_3^{2+} = tris(2,2-bipyridine)ruthenium(II)]/TPrA$ (TPrA = tri-n-propylamine), at the electrode surface, only luminophore species can be regenerated, whereas the coreactant is consumed via electrochemicalchemical reactions. Table 2.1 lists typical coreactant ECL systems for which the ECL mechanisms have been well studied. In situ generated coreactant intermediates, as indicated by their standard redox potentials, are either strong reducing agents (in oxidative-reduction ECL) or strong oxidizing agents (in reductive-oxidation ECL).

Another difference between annihilation and coreactant ECL is that, in annihilation ECL, all starting species can be regenerated after light emission, while in coreactant ECL, only luminophore species can be regenerated and the coreactant is consumed via the ECL reactions [16].

A good ECL coreactant must met a number of criteria, which include solubility, stability, electrochemical properties, kinetics, quenching effect, ECL background. Of these, the most important factor is the electrochemical properties of the coreactant. The coreactant should be easily oxidized or reduced with the luminophore species at or near the electrode and undergo a rapid chemical reaction to form an intermediate that has sufficient reducing or oxidizing energy to react with the oxidized or reduced luminophore to form the excited state.

Reaction process	Oxidative-reduction ECL	Reductive-oxidation ECL
Redox reactions at electrode	$R - e^- \longrightarrow R^{\bullet+}$ $C - e^- \longrightarrow C^{\bullet+}$	$R + e^- \longrightarrow R^{\bullet-}$ $C + e^- \longrightarrow C^{\bullet-}$
Homogeneous chemical reactions	$R^{\bullet+} + C \longrightarrow R + C^{\bullet+}$ $C^{\bullet+} \longrightarrow C^{inl}_{red}$ $C^{inl}_{red} + R \longrightarrow R^{\bullet-} + P$	$R^{\bullet-} + C \longrightarrow R + C^{\bullet-}$ $C^{\bullet-} \longrightarrow C^{inl}_{ox}$ $C^{inl}_{ox} + R \longrightarrow R^{\bullet+} + P$
Excited state species formation	$R^{\bullet+} + R^{\bullet-} \longrightarrow R + R^*$ or $R^{\bullet+} + C^{inl}_{red} \longrightarrow R^* + P$	$R^{\bullet+} + R^{\bullet-} \longrightarrow R + R^*$ or $R^{\bullet-} + C^{inl}_{ox} \longrightarrow R^* + P$
Light emission	$R^* \longrightarrow R + h\nu$	$R^* \longrightarrow R + h\nu$

Table 2.2: General mechanisms of coreactant ECL systems

Where R is the luminophore, C is teh coreactant, C^{inl} is the intermediate coreactant with subscript "red" for reducing agent and "ox" for oxidizing agent and P is the associated product of the reaction.

As summarized in Table 2.2, four processes generally are involved in all coreactant ECL systems toward the light emission, namely, (a) redox reactions at electrode, (b) homogeneous chemical reactions, (c) excited state species formation, and (d) light emission. Depending on the nature of the working electrode and the redox potential of the coreactant, both heterogeneous and homogeneous redox reactions of coreactant are possible. The formation of excited state species also has two general routes: the classical ion annihilation and the reaction involving coreactant intermediate.

2.3.1 Annihilation vs Coreactant

Coreactant systems for ECL offer several advantages with respect to the ion annihilation systems. The advantages listed below contain some examples that justify the reason that, nowadays, most of the commercial available ECL systems are based on coreactant reactions.

1. The use of a coreactant can make ECL possible even for some fluorescent compounds that have only a reversible electrochemical reduction or oxidation.

2. Even with solvents for ECL that have a narrow potential window so that only a reduced or oxidized form of a luminophore can be produced, e.g., $tris(2,2bipyridine)ruthenium(II)$, $Ru(bpy)^{2+}_3 (bpy =$

$2,2'$*bipyridine*), in aqueous solutions, it is still possible to generate ECL by use of a coreactant.

3. When the annihilation reaction between oxidized and reduced species is not efficient,the use of a coreactant may produce more intense ECL.

2.3.2 Typical Coreactant ECL Systems

Although there are a wide variety of molecules that exhibit ECL, the overwhelming majority of publications concerned with coreactant ECL and its analytical applications are based on chemistry involving $Ru(bpy)_3^{2+}$, or closely related analogues as the emitting species [17], because of their excellent chemical, electrochemical, and photochemical properties even in aqueous media and in the presence of oxygen. As a result, much of this section concerns $Ru(bpy)_3^{2+}$ /coreactant ECL systems.

Oxalate System

This was the first account of coreactant ECL system reported in the literature by Bards group in 1977 [18], and is a classical example of oxidative-reduction ECL. The ECL mechanism of this system was proposed to be as in the Equations 2.13 to 2.19 [19] [20].

$$Ru(bpy)_3^{2+} - e^- \longrightarrow Ru(bpy)_3^{3+} \tag{2.13}$$

$$Ru(bpy)_3^{3+} + C_2O_4^{2-} \longrightarrow Ru(bpy)_3^{2+} + C_2O_4^{\bullet -} \tag{2.14}$$

$$C_2O_4^{\bullet -} \longrightarrow CO_2^{\bullet -} + CO_2 \tag{2.15}$$

$$Ru(bpy)_3^{3+} + CO_2^{\bullet -} \longrightarrow Ru(bpy)_3^{2+*} + CO_2 \tag{2.16}$$

$$Ru(bpy)_3^{2+} + CO_2^{\bullet -} \longrightarrow Ru(bpy)_3^{+} + CO_2 \tag{2.17}$$

$$Ru(bpy)_3^{3+} + Ru(bpy)_3^{+} \longrightarrow Ru(bpy)_3^{2+} + Ru(bpy)_3^{2+*} \tag{2.18}$$

$$Ru(bpy)_3^{2+*} \longrightarrow Ru(bpy)_3^{2+} + h\nu \tag{2.19}$$

Firstly, the $Ru(bpy)_3^{2+}$ is oxidized at the electrode to the $Ru(bpy)_3^{3+}$ cation. This species is then capable of oxidizing the oxalate ($C_2O_4^{2-}$) in the diffusion layer close to the electrode surface to form an oxalate radical anion ($C_2O_4^{\bullet -}$). This breaks down to form a highly reducing radical anion ($CO_2^{\bullet -}$, $E^0 = -1.9V$ vs normal hydrogen electrode (NHE) [21]) and carbon dioxide. The reducing intermediate then either reduces the $Ru(bpy)_3^{2+}$ complex back to the parent complex in an excited state, or reduces $Ru(bpy)_3^{2+}$

to form $Ru(bpy)_3^{2+}$ that reacts with $Ru(bpy)_3^{2+}$ to generate the excited state $Ru(bpy)_3^{2+}$, which emits light with $\lambda_{max} \approx 620nm$. In aqueous solutions, the ECL intensity of the $Ru(bpy)_3^{2+}$ /oxalate system has been reported to have a maximum at pH 6 [19], and also to be essentially constant from pH 48 [22] [23] at macro-electrodes and from pH 58 at microelectrodes [24].

Peroxydisulfate System

This was the first example of so called "reductive-oxidation" coreactant ECL system reported in the literature [24][25]. Because $Ru(bpy)_3^{2+}$ is unstable in aqueous solutions and $(NH_4)_2S_2O_8$ has a low solubility in $MeCN$ solutions, the $MeCNH_2O$ mixed solutions were chosen to produce intense ECL emission [25]. Equations 2.20 to 2.26 summarize the possible pathways for the production of $Ru(bpy)_3^{2+}$ when $S_2O_8^{2-}$ is used as the coreactant, in which the strongly oxidizing intermediate $S_2O_4^{\bullet -}$, generated during reduction of $S_2O_8^{2-}$, has a redox potential of $E^0 > 3.15V$ vs. saturated calomel electrode (SCE) [26].

$$S_2O_8^{2-} e^- \longrightarrow S_2O_8^{\bullet 3-} \tag{2.20}$$

$$Ru(bpy)_3^{2+} + e^- \longrightarrow Ru(bpy)_3^{+} \tag{2.21}$$

$$Ru(bpy)_3^{+} + S_2O_8^{2-} e^- \longrightarrow Ru(bpy)_3^{2+} + S_2O_8^{\bullet 3-} \tag{2.22}$$

$$S_2O_8^{\bullet 3-} \longrightarrow S_2O_4^{2-} + S_2O_4^{\bullet -} \tag{2.23}$$

$$Ru(bpy)_3^{+} + S_2O_4^{\bullet -} \longrightarrow Ru(bpy)_3^{2+*} + S_2O_4^{2-} \tag{2.24}$$

$$Ru(bpy)_3^{2+} + S_2O_4^{\bullet -} \longrightarrow Ru(bpy)_3^{3+} + S_2O_4^{2-} \tag{2.25}$$

$$Ru(bpy)_3^{+} + Ru(bpy)_3^{3+} \longrightarrow Ru(bpy)_3^{2+*} + Ru(bpy)_3^{2+} \tag{2.26}$$

It is believed that persulfate ion is a coreactant of $Ru(bpy)_3^{2+}$ ECL as well as an effective quencher of the excited state $Ru(bpy)_3^{2+}$ [34,45]. As a result, the ECL intensity of the $Ru(bpy)_3^{2+}$ /S2O2 8 system was found to be a function of $S_2O_8^{-2}$ concentration, and for 1 mM $Ru(bpy)_3^{2+}$ solution the maximum ECL intensity was obtained at 1520 mM $S_2O_8^{2-}$ [25].

Luminol/Hydrogen Peroxide System

The ECL reaction of luminol (5-amino-2,3-dihydro-1,4-phthalazinedione) with hydrogen peroxide in alkaline medium is similar to the chemical luminescence of luminol triggered by chemical oxidation [27]. The general accepted mechanism is shown in the Figure 2.2. In alkaline solution luminol deprotonates to form an anion, which then undergoes electrochemical oxidation to produce a diazaquinone. This species is further oxidized by peroxide or super-oxide to give 3-aminophthalate in an excited state that emits light at, approximately, 425 nm.

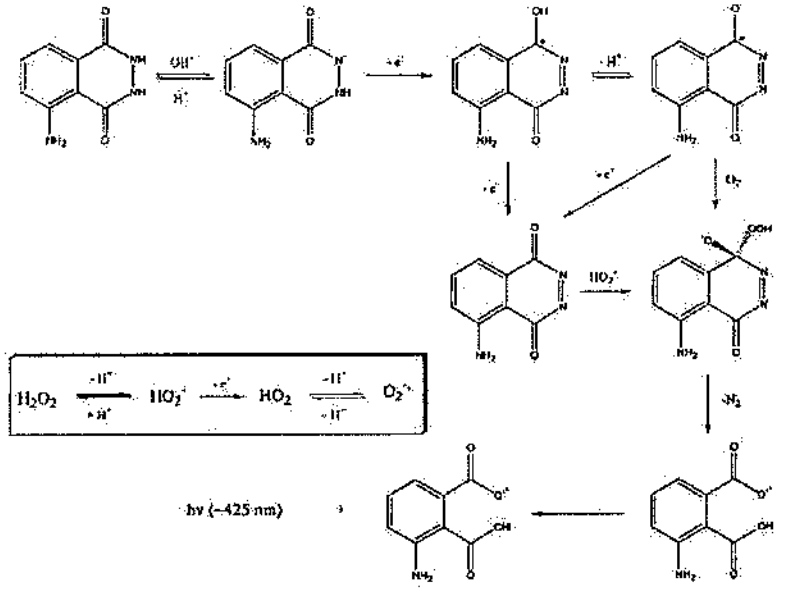

Figure 2.2: Luminol/Hydrogen peroxide system mechanism[28]

Chapter 3

The Ruthenium/Tri-n-propylamine (TPrA) and Other Amines System

3.1 Introduction

In 1987, Noffsinger and Danielson first studied the chemiluminescence of $Ru(bpy)_3^{2+}$ with aliphatic amines [29]. In 1990, Leland and Powell reported the ECL of $Ru(bpy)_3^{2+}$ with TPA as a coreactant [30], and Blackburn et al. soon developed $Ru(bpy)_3^{2+}$ ECL immunoassays and DNA probe assays using TPA as coreactant and $Ru(bpy)_3^{2+}$ as the label [31]. $Ru(bpy)_3^{2+}$ labels coupled with TPA have also been used for the detection of DNA derived from Bacillus[32]. The mechanism of $Ru(bpy)_3^{2+}$/TPA ECL system was studied in detail by several groups. The reaction procedures for the production of the excited state of $Ru(bpy)_3^{2+}$ are shown in Figure 3.1 and 3.3[33]. An EPR spectrometer equipped with a continuous flow assembly has also been used to monitor the intermediate species formed during the chemiluminescent reactions of $Ru(bpy)_3^{2+}$ and two opiate alkaloids [34]. It has spectroscopically shown that the reaction pathways outlined in Scheme 2 can be accurately extended beyond the devised $Ru(bpy)_3^{2+}$/TPA mechanism. These studies show that the direct electrochemical oxidation of TPA on the electrode plays an important role when the concentration of $Ru(bpy)_3^{2+}$ is much lower than that of TPA [33, 35, 36]. Some surfactants [37, 38] and fluorinated alcohols [39] can promote the oxidation of TPA and dramatically increase sensitivity. In contrast, some phenols, hydroquinones, catechols, and benzoquinones can

quench ECL of $Ru(bpy)_3^{2+}$/TPA [40, 41].

3.2 Main Reaction

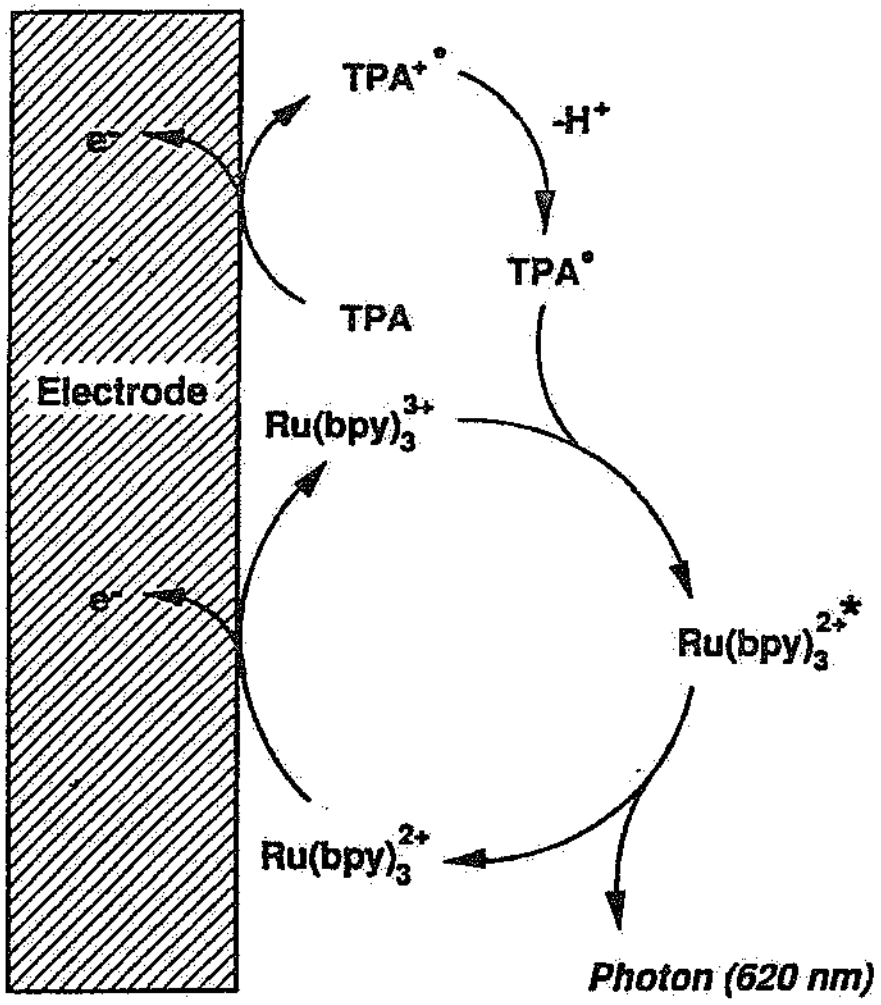

Figure 3.1: TPrA/ruthenium main reaction

Figure 3.1 presents, schematically, the main ECL reactions for the TPrA system. The reactions are written below.

$$Ru(bpy)_3^{2+} - e^- \longrightarrow Ru(bpy)_3^{3+} \tag{3.1}$$

$$TPrAH^+ - H^+ \longrightarrow TPrA \tag{3.2}$$

$$TPrA - e^- \longrightarrow TPrA^{\bullet+} \tag{3.3}$$

$$TPrA^{\bullet+} - H^+ \longrightarrow TPrA^{\bullet} \tag{3.4}$$

$$Ru(bpy)_3^{3+} + TPrA^{\bullet} \longrightarrow Ru(bpy)_3^{2+*} + P1 \tag{3.5}$$

$$Ru(bpy)_3^{2+*} \longrightarrow Ru(bpy)_3^{2+} + h\nu \tag{3.6}$$

The mechanism presently presented in the literature and in some of the ECL instrument manufacturern Websites including the technical application notes is often simplified. Generally, the ECL emission of this system as a function of applied potential consists of two waves. The first occurs with the direct oxidation of TPrA at the electrode, and this wave is often merged into the foot of the second wave when relatively high concentrations of $Ru(bpy)_3^{2+}$ (millimolar) are used.

The direct oxidation of TPrA at an electrode plays an important role in the ECL process of the $Ru(bpy)_3^{2+}$ /TPrA system and varies with the electrode material and its surface hydrophobicity. For example, in the presence of added small amounts of halide species that could inhibit the growth of the oxide surface on Pt and Au electrodes or low concentrations of surfactants (nonionic and ionic) that could increase the hydrophobicity of the electrode, the oxidation rate of TPrA and hence the ECL intensity increased significantly [42, 43]. electrochemical windows. The ECL intensity for the first and the second waves was also found to be proportional to the concentration of TPrA species over a very large dynamic range (up to 0.10 M) [44, 45, 46]. Dissolved O_2 could influence the ECL intensity when low concentrations (smaller than 20 mM) of TPrA are used, which is particularly remarkable for the first ECL wave. This behavior can be readily explained on the basis of the ECL mechanisms described in Figures 3.1 and 3.3: A large excess of intermediate reducing radicals ($TPrA^{\bullet}$) was produced at high [TPrA], and the dissolved O_2 within the ECL reaction layer was completely reduced by these radicals and exerted no quenching effect on the emission. At low [TPrA], however, coreactant oxidation generated a relatively small amount of reducing intermediates, and O_2 acted as an interceptor, destroying the intermediates before they participated in the ECL pathways, which led to the obvious reduction of the emission intensity. In the latter case, the less efficient initial ECL route was more significantly affected [47]. Up to 2.5 V vs Ag/AgCl anodic potential limit can be reached for neutral aqueous ECL systems at the deposited boron-doped diamond (BDD) electrode. Three ECL waves at 1.2, 2.0, and 2.3 V vs Ag/AgCl for $Ru(bpy)_3^{2+}$ /TPrA, which correspond to the oxidation reaction of $Ru(bpy)_3^{2+}$ at the electrode and homogeneous catalytic oxidation

of TPrA with electrogenerated $Ru(bpy)_3^{3+}$, the direct oxidation of TPrA at the electrode, and the electrode oxidation of propylamine formed by preceding dealkylation of TPrA, respectively, were observed. The wide potential window in aqueous solution and the high stability for ECL due to the low adsorption property for reaction products make such a diamond electrode very promising for ECL production of amines with high oxidation potentials. Hydroxyl radical $(OH)^{\bullet-}$ related ECL reactions for $Ru(bpy)_3^{2+}$ coreactant (ascorbic acid and alcohols) systems at BDD electrode were also observed in the extremely positive potential region (¿2.6 V with a peak potential at 3.7 V vs Ag/AgCl) [48]. It is believed that the coreactant radical was formed through the hydrogen abstraction reaction with the $(OH)^{\bullet-}$ generated during the oxygen evolution reaction. Such behavior was not found at GC or Pt electrode.

The formation of OH^-, at the BDD electrode in the high-potential region (bigger than 2.6 V vs Ag/AgCl) was confirmed previously by ESR measurement with the spin-trap method [49]. The ECL intensity of the $Ru(bpy)_3^{2+}$ /TPrA system also strongly depends on the solution pH[50], with dramatic increases at pH lower than 5.5 and a maximum value at pH 7.5. The exact reason remains unclear, but this may be associated with the deprotonation reactions of $TPrAH^+$ and $TPrA^+$ shown in Figures 3.1 and 3.3 as well as the stability of the intermediates formed. Solubility decrease of TPrA at high pH could be another reason why TPrA produces the highest ECL intensity at pH 7.5. A recent study regarding the influence of the nature, concentration, and pH of buffer on the rate-determining step of $Ru(bpy)_3^{2+}$ /tertiary aliphatic amine systems revealed that deprotonation of the ammonium species is the rate-determining step at pH ¡5, whereas deprotonation of radical cations is the rate-determining step at pH ¿5 [51]. Usually, pH values higher than 9 should not be used, because $Ru(bpy)_3^{3+}$ generated at the electrode could react with hydroxide ions to produce a significant ECL background signal.

The electrochemistry, UV-vis absorption, PL of $Ru(bpy)_3^{2+}$, and its ECL withTPrA have been reported in a series of hydroxylic solvents such as fluorinated and non-fluorinated alcohols and alcohol/water mixtures [52]. Blue shifts of up to 30 nm in PL and ECL emission wavelength maximums were observed compared to a $Ru(bpy)_3^{2+}$ /H2O standard due to interactions of the polar excited state [i.e., $Ru(bpy)_3^{2+*}$] with the solvent media. Dramatic increases in ECL efficiencies ranging from 6- (in 5% BuOH) to 270-fold (in 30% 2,2,2-trifluoroethanol) were seen in mixed alcohol/water solutions compared to $Ru(bpy)_3^{2+}$ (0.1 M)/TPrA (40 mM) in water.

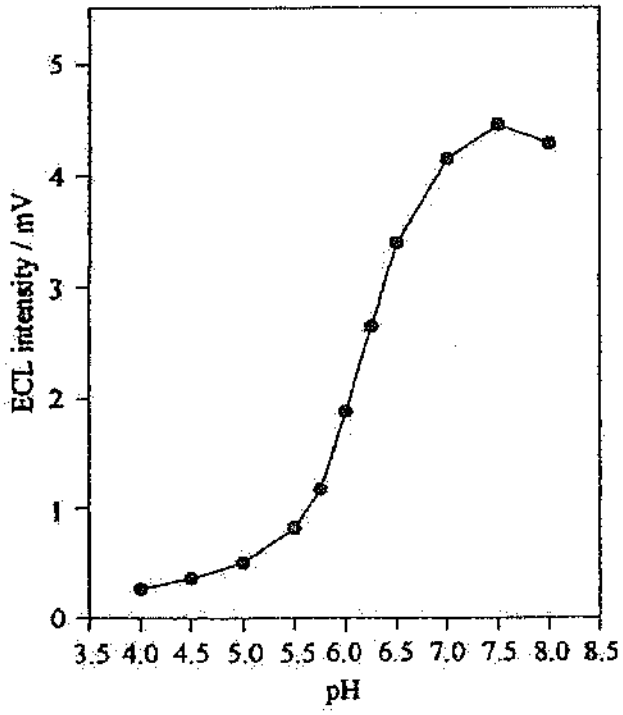

Figure 3.2: pH effect on the ECL intensity

3.3 Side Reactions

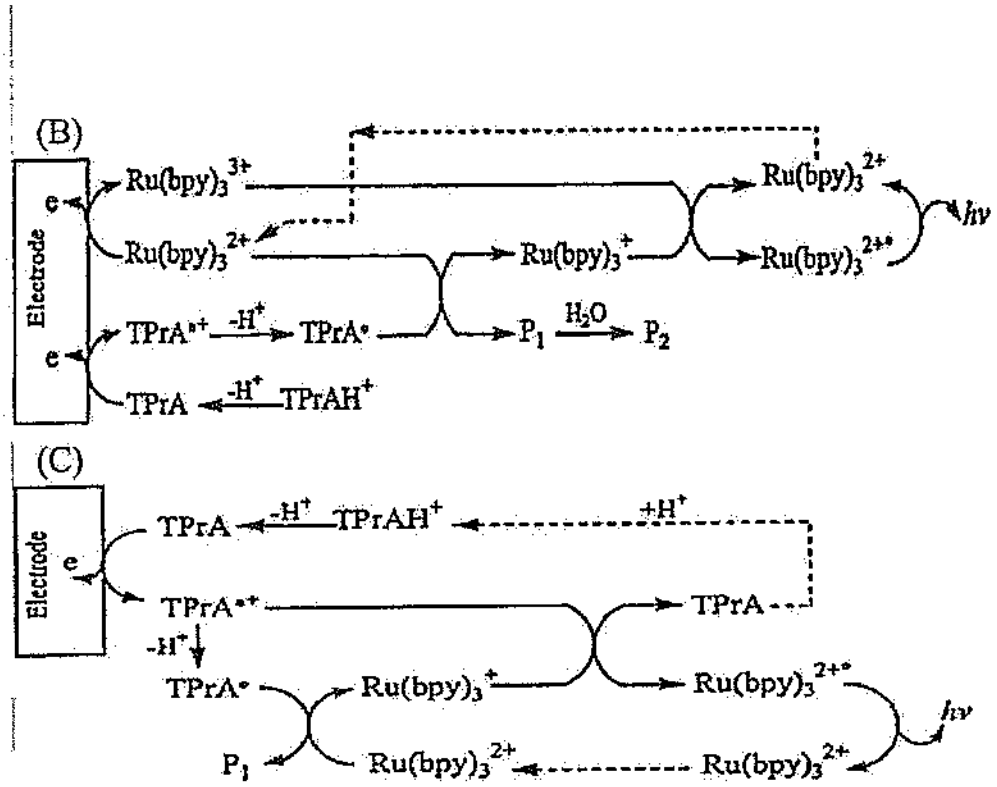

Figure 3.3: TPrA secondary reactions

Figure 3.3 represents the secondary reactions of the TPrA system. The second wave appears where $Ru(bpy)_3^{2+}$ is oxidized [45, 53]. Both waves are associated with the emission from $Ru(bpy)_3^{2+*}$. The relative ECL intensity from the first wave is significant, particularly in dilute $Ru(bpy)_3^{2+}$ solutions (less than approximately micromolar) containing, approximately, 0.1 M of TPrA. Thus, the bulk of the ECL signal obtained in this system with low concentrations of analytes, as in immunoassay and DNA probes with $Ru(bpy)_3^{2+}$ as an ECL label, probably originates from thefirst ECL wave. Figure 3.1 summarizes the mechanism of the first ECL wave, where the cation radical species $TPrA^+$ formed during TPrA oxidation is a sufficiently stable intermediate with a half-life of 0.2 ms that it can oxidize $Ru(bpy)_3^{2+}$ [formed from

the reduction of $Ru(bpy)_3^{2+}$ by $TPrA^{\bullet}$ free radical] to give $Ru(bpy)_3^{2+*}$. The mechanism of the second ECL wave follows the classic oxidative-reduction coreactant mechanism, where oxidation of TPrA generates a strongly reducing species TPrA. (EP1/TPrA -1.7 V vs SCE). This oxidation can be via a catalytic route, where electrogenerated $Ru(bpy)_3^{3+}$ reacts with TPrA, as well as by direct reaction of TPrA at the electrode described by Figure 3.3. The catalytic route involving homogeneous oxidation of TPrA with $Ru(bpy)_3^{3+}$ is shown in Figure 3.4.

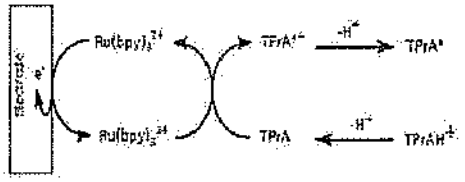

Figure 3.4: Catalytic route

The contribution of this process to the overall ECL intensity depends upon the $Ru(bpy)_3^{2+}$ concentration and is small when relatively low concentrations of $Ru(bpy)_3^{2+}$ are used.

3.4 Other Amine Systems

Similar to the case of TPrA, a wide range of amine compounds can be used as coreactants and take part in ECL reactions with $Ru(bpy)_3^{2+}$. Because amine groups are prevalent in numerous biologically and pharmacologically important compounds including amino acids and peptides, $Ru(bpy)_3^{2+}$/amine coreactant ECL forms the basis of a large number of biorelated species detection and determination. Several workers have tried to correlate the coreactant ECL efficiency with the amine structure. Although there are no strict rules governing ECL activity in amines, in general, the ECL intensity increases with the amine order. Primary amines with the lowest intensity, after secondary amines, then tertiary amines.Hence, tertiary amines have the lowest detection limits.

The amine should have a hydrogen atom attached to the R-carbon, so that upon oxidation newly formed radical cation species can undergo a deprotonation process to form a strongly reducing free radical species.

Also, the nature of substituents attached to nitrogen or R-carbon on an amine molecule can affect the ECL activity. In general, electron-withdrawing substituents tend to cause a reduction of ECL activity, and electron-donating groups have the opposite effect. Aromatic amines, aromatic substituted amines, and amines with a carbon-carbon double bond that can conjugate the radical intermediates consistently give a very low ECL response. Note that aromatic amines may also quench the emission of the $Ru(bpy)_3^{2+*}$ complex, further reducing the ability of these compounds to give an ECL response. Furthermore, amines that have other functional groups that are more readily oxidised than the nitrogen atom may take part in alternative, ultimately non-chemiluminescent, reactions. The ECL reaction mechanism of $Ru(bpy)_3^{2+}$ with six tertiary aliphatic amines, namely, tri-n-butylamine (TBnA), tri-isobutylamine (TisoBuA), TPrA, methyl-din-propylamine (MeDPrA), triethylamine (TEtA), and trimethylamine (TMeA), in aqueous solution was examined using fast potential pulses at carbon fiber microelectrodes and with simulation techniques with the aim to obtain information on the E^0 value of the amine redox couples [91].

Despite its exclusive popularity, TPA has some disadvantages, such as toxicity and volatility. In 2007, a new environmentally friendly coreactant 2-(dibutylamino)ethanol (DBAE) was reported [102]. The ECL intensity of the $Ru(bpy)_3^{2+}$/DBAE system at Au and Pt electrodes was found to be approximately 10 and 100 times greater than that of the commonly used $Ru(bpy)_3^{2+}$/TPrA system, respectively, when $25mM$ of each coreactant was used in the presence of $0.10M$ phosphate buffer (pH 7.5). At the glassy carbon (GC) electrode, however, the ECL performance of this system was poor; the intensity of ECL first increased with the concentration of DBAE up to $3mM$ and then leveled off. The GC enhancement of DBAE was attributed to the catalytic effect of hydroxyethyl group toward the direct oxidation of DBAE at the electrode. This suggests that not all electron-withdrawing substitutive such as the hydroxyethyl group in the current case cause GC efficiency decrease. Compared to $Ru(bpy)_3^{2+}$/TPrA, the $Ru(bpy)_3^{2+}$/DBAE system exhibits a wider dynamic range and has a lower detection limit for $Ru(bpy)_3^{2+}$ at the Au electrode and very sensitive ECL responses at Pt electrode. As a result, DBAE is a promising coreactant for $Ru(bpy)_3^{2+}$ ECL immunoassays and DNA probe assays.

Chapter 4

ECL: State of the Art

In this chapter the latest solutions in terms of ECL are briefly analyzed and discussed. A first distinction has been made through the luminophore involved in the reaction (mainly $Ru(bpy)_3^{2+}$ or luminol); different innovative electrode materials (gold nanoparticles, carbon nanotubes), and their response, have been then considered. The absence of a light source in ECL [64] frees this method from light interferences and opens unique avenues for sensing, especially when combined with the wide variety of micro and nanomaterials developed nowadays. Because of this feature, traditional ECL methods have earned renewed attention when used in combination with nanotechnology and a great number of recent articles on this subject is focused on the development of chemical and biological ECL sensors that generally exhibit improved characteristics (sensitivity, linear response, detection limits) for the determination of trace analytes. As already discussed, ECL can be produced by several distinct approaches and the two common luminophores utilized so far are the $Ru(bpy)_3^{2+}$ and the luminol.

4.1 Materials

4.1.1 Thin Films

Unlike luminol which is consumed during the ECL reaction, $Ru(bpy)_3^{2+}$ can be regenerated. Thus, it can be immobilized onto an electrode surface and reused in a thin-film sensor platform [65]. A $Ru(bpy)_3^{2+}$ containing thin-film sensor produces a smaller heavy metal waste, requires a less complicated pumping system, and reduces costs compared with a solution-based sensing method [66]. Nafion is an effective ion exchanger for $Ru(bpy)_3^{2+}$ and

has been used for $Ru(bpy)_3^{2+}$ immobilization [67]. However, a pure Nafion film sensor is far from ideal due to slow mass transfer of the analyte, instability of the films in organic solvents and partitioning into hydrophobic regions of the film. Nevertheless, $Ru(bpy)_3^{2+}$ incorporation into Nafion has seen some success because of both ion-exchange and hydrophobic interactions [68]. Langmuir-Blogdett films and self-assembled monolayers (SAM) have largely failed in the case of $Ru(bpy)_3^{2+}$ based sensors because the high potentials required to produce an ECL signal are detrimental to these films [68]. So far, two effective ECL films are sol-gel and polymer films.

Sol-gels

Many recent successes with thin-film ECL sensor platforms have been achieved with sol-gels. Pastore et al. successfully embedded $Ru(bpy)_3^{2+}$ inside silica glass thin-films deposited via a sol-gel dipping procedure on K-glass conducing substrates. The film was transparent, chemically inert, physically rigid, and stable for over one thousand experiments [66]. Dong et al. reported a composite film of Eastman-AQ55D cation-exchange polymer and silica sol-gel as an effective means for direct $Ru(bpy)_3^{2+}$ immobilization. Eastman-AQ55D has excellent ion-exchange properties and is more hydrophobic than Nafion, resulting in better retention of the hydrophobic $Ru(bpy)_3^{2+}$ ion and thus a more stable sensor [69].

Other sensing platforms have been built combining sol-gels and Nafion films. For instance, Lee et al. have reported sol-gel-derived $TiO_2 - Nafion$ composite films for effective immobilization of $Ru(bpy)_3^{2+}$ at an electrode surface. This ECL sensor showed improved ECL sensitivity as compared with ECL sensors based on pure Nafion films. The reason was ascribed to larger pores and thus faster diffusion of analytes into the film [65]. Thereafter, the same group developed mesoporous films of $V_2O_5/Nafion$ composites as effective materials to immobilize $Ru(bpy)_3^{2+}$.

It was found that the composite film with 80% Nafion content had the largest pore diameter (4.19 nm) and highest ECL yields with tripropylamine (TPrA). The greater sensitivity was the result of not only the large pores that offered rapid analyte diffusion, but also the relatively high conductivity of V_2O_5. Based on these advantages, this ECL sensor exhibited a higher ECL response of approximately two orders of magnitude and a lower (around one order of magnitude) detection limit for TPrA (10 nM) compared with ECL sensors based on $SiO_2/Nafion$ and $TiO_2/Nafion$ [70].

The growing trend toward the use of nanotechnology has also made its way into the formation of thin-film sensing platforms. Xu and coworkers have created three-dimensional sensing platforms by depositing gold on silica nanoparticle (SNP) templates. Using hydrofluoric acid (HF) to dissolve the nanoparticles, a macroporous gold structure with a large active surface area and excellent conductivity (enhanced by the interconnected macroporous structure) was left behind, onto which a $ZrO_2/Nafion$ film containing $Ru(bpy)_3^{2+}$ was deposited. Compared with flat surfaces, increased $Ru(bpy)_3^{2+}$ loading was achieved with this configuration, yielding high sensitivity [68].

Metallopolymers

Metallopolymers, or polymers containing metal cores, provide an additional method for ECL reagent immobilization since they can be directly deposited onto an electrode. Polymers which contain a $Ru(bpy)_3^{2+}$ core (e.g., Figure 4.1) can produce ECL by a mechanism similar to $Ru(bpy)_3^{2+}$. Dennany et al. have shown in their studies that the overall efficiency of the ECL reaction for the metallopolymer film is almost four times higher than the highest value obtained for the same complex dissolved in solution, due mainly to protection from oxygen quenching and competing side reactions. The metallopolymer used in these studies is shown in Figure 4.1, and it is based on both annihilation and co-reactant mechanisms [71].

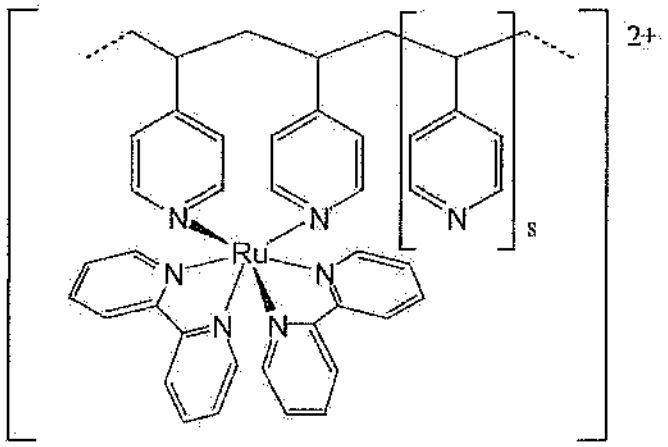

Figure 4.1: $[Ru(bpy)_2(PVP)10]^{2+}$, PVP = poly(4-vinylpyridine)

In an additional report by Lee at al., $Ru(bpy)_3^{2+}$ was modified with $Si(OMe)_3$ groups on each ligand (Figure 4.2). After hydrolysis of the silicate groups, a thin, porous polymer film was immobilized on an indium-tin oxide (ITO) electrode. The reason for choosing ITO as the electrode material was that the hydroxyl groups on its surface would also bound with the modified $Ru(bpy)_3^{2+}$ through silicon and oxygen bonds. The film had a long-term stability, even after long-term exposure to acetonitrile [72].

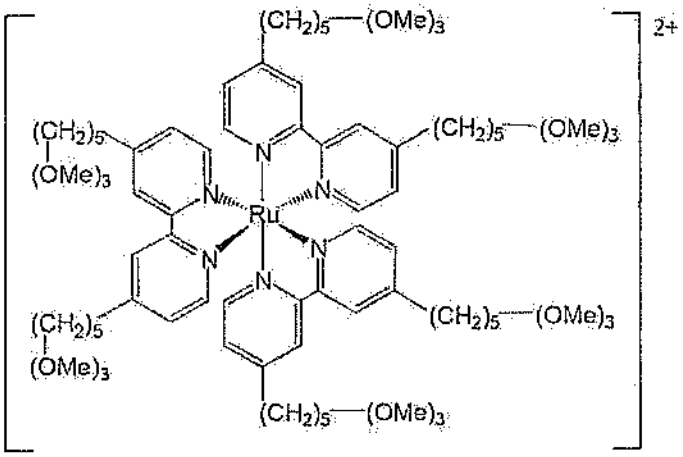

Figure 4.2: $Si(OMe)_3 - modifiedRu(bpy)^{2+}$

4.1.2 Electrode Arrays

The benefit of having an array of microelectrodes rather than a single electrode is that different data can be collected simultaneously, thus arrays can reduce interferences through data processing [73]. Furthermore, they can allow simultaneously determinations of multiple analytes [74]. In the case of the electrochemical signal produced by an array, individual electrodes are indistinguishable. In contrast, the ECL signals for individual electrodes can be read separately with a CCD camera or an optical fibre bundle [75]. Sojic et al. created a microelectrode array by coating conical glass cores with ITO then insulating the surface, except for the apex of the tips, with electrophoretic paint. ECL signals from the submicron sensors for both $Ru(bpy)_3^{2+}$ /TPrA [75] and $luminol/H_2O_2$ [73] were individually read with optical fibers. Although the electrodes could be read individually they could not be controlled individually, and thus only one analyte could be detected at a time [72]. Otherwise, Marquette and coworkers modified GC foil electrodes in order to

detect multiple analytes simultaneously. The enzymatic production of H_2O_2 was detected for all analytes, but at different areas of the electrode [76]. Oxidative enzymes were spotted on the foil electrode and non-covalently immobilized. Luminol ECL was used to detect H_2O_2 that was enzymatically produced in the presence of the respective substrates [74].

4.1.3 Microfluidics

The relatively new field of microfluidics has advantages of flexible cell designs, low cost, miniaturization and automation. However, the most sensitive detectors for these devices, such as laser-induced fluorescence (LIF) and mass spectrometry (MS), are bulky and expensive. Electrochemical detection systems are generally less expensive and more spatially compact, but they are not as sensitive as the above mentioned detectors. ECL sensing platforms may play an important role in this area since they show a sensitivity comparable to the one of more expensive LIF and MS detection systems, but they have the same size advantages of electrochemical systems [77]. A recent example of ECL detection in microfluidics was reported by Pittet et al. who detected hydrogen peroxide with luminol ECL. Printed circuit board (PCB) electrodes were used in this example, which can be fabricated inexpensively in large-scale production [78].

Crooks et al. have also developed a two-electrode microfluidic device where targets are detected electrochemically at the cathode (Equation 4.1), and then reported via ECL at the anode (Equation 4.2). Through this method, it is not necessary for the target analyte to have the capacity to react with $Ru(bpy)_3^{3+}$ to produce ECL, it only needs to be redox active.

$$Cathode: O + e^- \longrightarrow R \tag{4.1}$$

$$Anode: Ru(bpy)_3^{2+} \longrightarrow Ru(bpy)_3^{3+} + e^- \tag{4.2}$$

Since the two working electrodes are in electrochemical communication and a charge balance must be maintained, the reaction at the cathode shown in Equation 4.1 creates the anodic reaction (Equation 4.2). TPrA, present in solution, is able to react with $Ru(bpy)_3^{3+}$ to produce ECL. The two channels are connected by an outlet. However, due to laminar flow, there is no bulk mixing [77]. The same group also reported a three-channel system where both the target analyte detection and the ECL reporting occur at the anode. Therefore, oxidation of the target competes with oxidation of $Ru(bpy)_3^{2+}$,

and its presence causes a decrease in ECL signal [79].

4.1.4 Nanomaterials in Recent ECL Sensors

Nanotechnology is defined as the fabrication of structures or devices on the atomic or molecular scale, but it also includes devices that are less than 100 nm in at least one dimension [80]. Nanomaterials encompass a broad range of materials, including nanoparticles, nanorods, nanocrystals, nanowires and nanotubes of virtually any chemical composition. Due to the small size, usually nanomaterials experience light scattering when used in optical measurements. However, this drawback can be completely eliminated in ECL determination since no radiation source is needed. Thus, the advantages of both nanomaterials and ECL can be fully exploited when an ECL sensor is made of nanomaterials. Nanomaterials can enhance sensitivity by increasing the surface area [81] or enhancing the conductivity [82] of a sensor platform. For instance, porous nanoparticles had been used to sequester high concentrations molecules of the ECL-producing agent, resulting in labels with greater luminescence [83]. QDs are nanoparticles that have their own intrinsic ECL-producing ability [84].

The following list present the some nanomaterials that are used in ECL systems.

1. Gold nanoparticles. Due to its biological compatibility, high conductivity and ability to bound with amines and thiol;
2. Platinum nanoparticles. Due to its high conductivity and electroactivity;
3. Magnetic nanoparticles, (Fe_3O_4). Due to the fact that these particles can be easy immobilized;
4. Silica nanoparticles. Due to its versatility;
5. Carbon nanotubes. Due to its conducting properties.

4.2 ECL Sensing Applications

4.2.1 Label Free Sensors

Ruthenium/Amines

The ability of $Ru(bpy)_3^{2+}$ to react with amines radicals to produce ECL makes it useful in detecting a variety of important analytes. Among them is guanine (G), the DNA base (Equations 4.4) [85]. Furthermore, $Ru(bpy)_3^{2+}$ can more easily react with single stranded (ss) DNA compared with double stranded (ds). Reported rates for the reaction shown in Equation 4.3 were $9 \times 10^3 M^{-1}s{-}1$ for ds calf thymus DNA and $2 \times 10^5 M^{-1}s{-}1$ for ss calf thymus DNA. This characteristic makes the ECL method particularly useful in detecting base mismatches [85]. Forster et al. used the metallopolymer to detect chemical damage to ds-DNA. DNA and the metallopolymer were deposited alternately using the layerby- layer method. The films were then incubated with styrene oxide to cause chemical damage. The group was able to detect 0.1% damage, or one base in one thousand [85]. Wang et al. used a previously reported CNT and Nafion composite film [86] in which $Ru(bpy)_3^{2+}$ was incorporated in order to detect DNA. DNA was non-specifically bound to the film, and again, ss-DNA gave a more intense ECL signal. By exposing the films to a boiling water bath for five minutes, native ds-DNA was denatured and the ECL signals produced before and after this treatment could be compared. In this way, single-base mismatch could be detected. In addition, the group found that adenine also was able to contribute to the ECL signal [87]. Chen and coworkers used their organically modified silica film with PSS-coated CNTs [88], to detect herring sperm DNA. The ability of guanine to oxidize and behave as a co-reactant in $Ru(bpy)_3^{2+}$ ECL (Equations 4.3 to 4.5) were also exploited in this flow-injection analysis sensor. A modest detection limit of $0.2 mgL^{-1}$ was achieved [88].

$$Ru(bpy)_3^{2+} \longrightarrow Ru(bpy)_3^{3+} + e^- \tag{4.3}$$

$$Ru(bpy)_3^{3+} + DNA(G) \longrightarrow Ru(bpy)_3^{2+} + DNA^{\bullet+}(GOD) \tag{4.4}$$

$$DNA^{\bullet+}(GOD) + Ru(bpy)_3^{3+} \longrightarrow OH^- + QD^{\star} \tag{4.5}$$

Lee and coworkers have used the TiO2/Nafion composite sensor [78] for determinations of phenothiazine derivatives in urine samples after HPLC separation. Phenothiazines are a group of compounds often used in antidepressant drugs. Therefore, monitoring them in bodily fluids is important in order to minimize toxicity risk. They contain aliphatic tertiary amines,

which allow their detection with $Ru(bpy)_3^{2+}$ based ECL sensors [89]. Zhang et al. have used a sensor composed of $Ru(bpy)_3^{2+}$ -doped silica nanoparticles immobilized at an electrode surface in a chitosan film to detect itopride (N-[4-[2-(dimethylamino)- ethoxy]benzyl]-3,4-dimethoxybenzamide hydrochloride) (Figure 4.2.1) [90]. Their sensor was similar to the one reported by Dong et al. for TPA determinations [69].

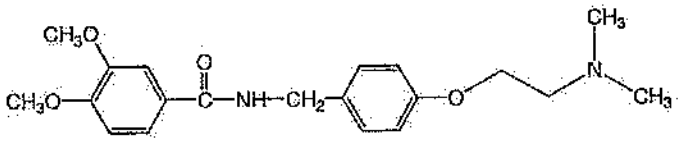

Figure 4.3: Itopride

Luminol

Luminol is useful for H_2O_2 determinations since reactions between luminol and H_2O_2 can produce ECL. H_2O_2 is also a product in many enzymatic reactions where substrates are oxidized by O_2. A prototypical example is the oxidation of glucose by the oxidoreductase enzyme, GOD (Equation 4.6). Thus H_2O_2 determinations can be an indirect method for the determination of biological compounds. Such is the case in the reports of Marquette et al., which described sensor arrays for simultaneous determinations of glucose, lactate, choline, glutamate, lysine and urate [80]. Oxidative enzymes were immobilized on the electrode surface where they could catalyse the production of H_2O_2, which would in turn react with luminol and produce ECL. Detection limits for the biological compounds were typically in the micromolar range [73, 75, 76].

$$\beta - D - glucose + O_2 \longrightarrow gluconicacide + H_2O_2 \tag{4.6}$$

Zhang and coworkers reported an example of luminol ECL produced by a galvanic cell to detect H_2O_2. Since galvanic cells require no external power source, cost and size of the sensor could be significantly reduced. ACu/Zn alloy produced the galvanic cells via the corrosion effect. In alkaline solution, the zinc dissolved from the alloy anodically, producing a potential of $+1.1V$ which is sufficient for ECL generation with luminol. The presence of H_2O_2 caused the chemiluminescence signal to increase. The detection limit

for hydrogen peroxide was $0.3mM$ [93]. Zhang and Zheng produced a sensor for pyrogallol (Py, Figure 4.2.1) that used luminol-doped silica nanoparticles to produce an ECL signal. The nanoparticles were immobilized at a graphite electrode in a chitosan film through which pyrogallol could diffuse and was electrochemically oxidized (Equation 4.7). The resulting pyrogallol radical could reduce oxygen to a anion radical which in turn reduces luminol to form AP^{*2-}, the ECL-producing product (Equations 4.8 and 4.9). ECL was therefore dependent on pyrogallol concentration. The reported detection limit was 1.0 nM [92].

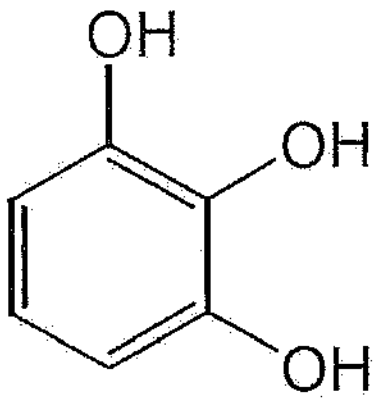

Figure 4.4: Pyrogallol

$$Py \longrightarrow Py^{\bullet} + e^{-} + H^{+} \tag{4.7}$$

$$Py^{\bullet} + O_2 \longrightarrow O^{\bullet -} + Py_{ox} \tag{4.8}$$

$$2O^{\bullet -} + luminol \longrightarrow AP^{*2-} + N_2 \tag{4.9}$$

4.2.2 ECL Labels

Molecular Labels

Kuwabara and coworkers reported that the ECL-producing ruthenium complex $Ru(phen)_3^{2+}$ was able to bind to the major groove of DNA. The result was that DNA added to a solution containing $Ru(phen)_3^{2+}$ and oxalate caused a decrease in ECL signal. The ruthenium complex was therefore used as a probe to determine the binding mode of certain anti-cancer drugs.

Evaluating the binding modes of drugs is an important step towards understanding the drug mechanism. If the drugs also preferred binding to the major groove, an increasing drug concentration would have a coinciding increasing ECL signal due to liberation of $Ru(phen)_3^{2+}$. On the other hand, if the drug only bound to the minor groove, concentration would have no effect [94]. Modified $Ru(bpy)_3^{2+}$ has been used as a molecular label in DNA and c-reactive protein (CRP) determinations by Miao and Bard. For DNA, a thiolmodified capture strands complimentary to the target were self assembled onto a gold electrode. The targets were labeled with $Ru(bpy)_3^{2+}$. The ECL signal resulting from a TPrA radical produced at strong potentials was then proportional to the target. Oxidation of the SAM was not addressed as a major problem, however, it was noted that the maximum ECL signal appeared at $+0.95V$ which is less positive than with free $Ru(bpy)_3^{2+}$. A similar method for CRP determination was reported in the same article. Biotinylated anti-CRP was immobilised on an avidin surface bound to a gold-thiol SAM in a sandwich-type assay. An anti-CRP probe was labeled with $Ru(bpy)_3^{2+}$, which gave an ECL signal proportional to the CRP concentration [95]. Zhang et al. reported a cocaine sensor, a $Ru(bpy)_3^{2+}$ modified aptamer which was immobilised to a gold electrode via the SAM method. The $Ru(bpy)_3^{2+}$ molecular probe at the end of a random coil did not give a strong ECL signal because of it distance from the electrode. However, after the binding of cocaine to the aptamer, the $Ru(bpy)_3^{2+}$ probe was in close proximity with the electrode, therefore giving a strong ECL signal in the presence of TPrA when a potential of $+0.8V$ was applied. It was also noted that potentials more positive than $+1.1V$ gave poor reproducibility due to the oxidation of the thiol SAM. The detection limit for this method was reported at 1 nM of cocaine [96]. Blum and coworkers used a derivative of luminol, N-(4-aminobutyl)-N-ethylisoluminol (ABEI) as a molecular probe for DNA determinations. Their capture DNA was modified with pyrrole on one end for the purposes of immobilisation. A pyrrole film was electrochemically deposited in the electrode with the pyrrole-modified DNA. The probe DNA was modified with biotin, as was the ABEI, therefore they could be connected through an avid-in bridge. It was shown that a complimentary probe gave a higher ECL signal in the presence of 1.3 mM H_2O_2 than a non-complimentary probe in a brief demonstration [97].

Micro and Nanoparticle Labels

Micro and nanoparticles that contain ECL-producing agents, primarily $Ru(bpy)_3^{2+}$, can also be used as labels in sensors. Because they contain

$Ru(bpy)_3^{2+}$ ions, the signals from these types of sensors can be greatly enhanced over molecular labels. Miao and Bard reported DNA [98] and CRP [99] determination with polystyrene microspheres (10 nm) containing the water-insoluble species $Ru(bpy)_3[B(C_6F_5)_4]_2$. Each microsphere contained approximately 7.5×10^9 molecules and was attached to a target DNA strand. The complimentary probe DNA was attached to a magnetic bead which could hybridise with the labeled target. The hybridised target DNA could then be magnetically separated from the single stranded targets [98]. The CRP sensor was a sandwich-type assay in which anti-CRP was attached to the polystyrene mircospheres as well and the magnetic beads. When these both bound to the CRP they could be magnetically separated to collect the polystyrene beads. The polystyrene microspheres were then dissolved in acetonitrile and $Ru(bpy)_3^{2+}$ was determined by ECL with TPA as the co-reactant. Detection limits of $1.0fM$ DNA were achieved and $10mgL^{-1}$ CRP. Zhan and Bard also reported a CRP sensor that used $Ru(bpy)_3^{2+}$ -containing liposomes (100 nM) as labels. The advantage of using liposomes rather than polystyrene microspheres was than the $Ru(bpy)_3^{2+}$ could be released with sodium chloride and a surfactant, which are more benign than acetonitrile. However, the detection limit was an order of magnitude higher at $100mgL^{-1}$ [100]. Fang and coworkers reportedly used $Ru(bpy)_3^{2+}$ doped silica nanoparticles as labels for DNA hybridisation determinations [83]. Captured DNA was immobilised at a polypyrrole modified platinum electrode, similarly to the method described in the previous section [97]. The silica nanoparticles were modified with complimentary target DNA which could hybridise with the DNA on the electrode surface. Unlike the method reported by Miao and Bard [98], the $Ru(bpy)_3^{2+}$ ions were not released. However, the co-reactant, oxalic acid, could penetrate the nanoparticles and allowed the production of ECL proportional to the amount of target DNA. A detection limit of $0.1pM$ was reported.

Chapter 5

COMSOL Model

5.1 Introduction

In this chapter the COMSOL model for the cyclic valtammetry test of the ruthenium-TpA system is presented. COMSOL is a software that solves differential equations using the finite elements method. The used version is 4.3b, and the module is electroanalysis, a subbranch of the electrochemistry module.

COMSOL has already been used on cyclic voltammetry models for ECL reactions, an example is the model ferrocyanide/ferricyanide redox equation [61].

5.2 Physics

The model contains a single 1D domain of length L, which is the maximum extent of the diffusion layer over the duration of the voltammetry experiment. A conservative setting for L is set to greatly exceed the diffusion layer thickness (Equation 5.1).

$$L = 6 \times \sqrt{(Dru \times 2 \times abs(Emin - Emax)/\bar{v})} \tag{5.1}$$

Here, D is the diffusion coefficient of the reactant, Emax and Emin are the potential limits of the test and v is the sweep rate of the cyclic voltammogram.

5.2.1 Domain Equations

We assume the presence of a large quantity of supporting electrolyte. This is inert salt that is added in electroanalytical experiments to increase the conductivity of the electrolyte without otherwise interfering with the reaction chemistry. Under these conditions, the resistance of the solution is sufficiently low that the electric field is negligible, and we can assume $\phi_l = 0$.

The Electroanalysis interface implements chemical transport equations for the reactant and product species of the redox couple subject to this assumption. The domain equation is the diffusion equation5.2 (Ficks 2nd law) to describe the chemical transport of the electroactive species.

$$\frac{dc_i}{dt} = \nabla.(D_i \nabla c_i) \tag{5.2}$$

Where c_i is the concentration of the specie and D_i is the diffusion coefficient of the specie.

5.2.2 Boundary Equations

The current density for this reaction is given by the electroanalytical Butler-Volmer equation for an oxidation5.3.

$$I_{oc} = nFK_0(c_{red} \exp \frac{(n - \alpha_c)F\eta}{RT} - c_{ox} \exp \frac{-\alpha_c F\eta}{RT}) \tag{5.3}$$

Where:

1. K_0 is the heterogeneous rate constant of the redox reaction;
2. α_c is the cathodic transfer coefficient;
3. η is the overpotential at the working electrode;
4. F is the Faraday's constant;
5. R is the Boltsmann's constant;
6. $c_{ox}; c_{red}$ are the concentrations of the oxidized and reducted species.

The overpotential is the difference between the applied potential and the equilibrium potential (formal reduction potential) of a redox couple of

species. According to Faradays laws of electrolysis5.4, the flux of the reactant and product species are proportional to the current density drawn.

$$-n \times N_i = \frac{v_i I_{oc}}{nF} \tag{5.4}$$

In the 1D approximation, the total current is related to the current density5.5 simply by multiplying by the electrode area A.

$$I_{el} = A \times I_{oc} \tag{5.5}$$

The reactions that will take place in the cell must be defined. For this model, only the main reaction of the TPrA system was implemented, in order to avoid unnecessary computational costs. Though the reactions were already presented in this work (chapter 3), they are repeated below.

$$Ru(bpy)_3^{2+} - e^- \longrightarrow Ru(bpy)_3^{3+} \tag{5.6}$$

$$TPrAH^+ - H^+ \longrightarrow TPrA \tag{5.7}$$

$$TPrA - e^- \longrightarrow TPrA^{\bullet +} \tag{5.8}$$

$$TPrA^{\bullet +} - H^+ \longrightarrow TPrA^{\bullet} \tag{5.9}$$

$$Ru(bpy)_3^{3+} + TPrA^{\bullet} \longrightarrow Ru(bpy)_3^{2+*} + P1 \tag{5.10}$$

$$Ru(bpy)_3^{2+*} \longrightarrow Ru(bpy)_3^{2+} + h\upsilon \tag{5.11}$$

5.3 Model Assumptions

This model is based on the following assumptions:

1. Only the main reaction is happening on the electrochemical cell.
2. The electrolyte does not offer significant ohmic resistance.
3. The system does not depend on the electrolyte pH.

5.4 COMSOL Implementation

5.4.1 Model Set-up

On building a COMSOL model, the primary and critical step is to define the inputs, parameters and geometry that will define the behavior of the whole system. An inappropriate chose of these terms leads to problems in compiling the model, singularities on the differential equations making the system non convergent and, in the worst case, provide results that are not according to the real system that the model is suppose to emulate. Each of the following sections explains the definitions used on the model of this work and how to perform changes on it, in case that one wishes to use this model to study other ECL systems.

Parameters

The parameters node on COMSOL is reached by right-clicking on the "Global Definitions" node and adding the node "Parameters". This node is used to organize the model, allowing any user to quickly understand what is being used and on which circumstances. For this work, all parameters are listed and briefly explained on Table 5.4.1.

The key parameters to the model of this work are the rate constants. They define the dynamic of all reactions that are happening on the ECL cell. These rate constants were obtained from R. Mark Wightman work[62].

One important detail to be highlighted is that, on the researched literature, the diffusion coefficients of the chemical species were not found. The solution was to set all these coefficients as the default COMSOL value, that can be observed on Tabel 5.4.1. The initial concentration of ruthenium and TPrA were also placed on the parameters, this makes the model easier to understand and also allow the user to perform "parametric sweeps" on the concentration, in order to observe how the system behaves for different concentrations of these species, if it is necessary and desirable.

Table 5.1: Model parameters

v	$1[V/s]$	voltammetric scan rate	Ref
T_amb	$300[K]$	room temperature	
V_therm	$T\_amb \times R\_const \times F\_const$	thermal voltage	
A	$R_e onst \times T_a mb/F_e onst$	reference potential without solution	
re	$10[mm]$	electorde radius	
Emin	$-1[V]$	start potential	
Emax	$1[V]$	switching potential	
c_ru	$0.1[mol/m^3]$	ruthenium initial concentrarion	
c_tpa	$1[mol/m^3]$	TPrA initial concentration	
Kr	$10^0[m^3/(mol \times s)]$	reaction constant for the reaction between the oxidized ruthenium and the reactive TPrA	[64]
Ke	$10^{7.2}[1/s]$	emission rate constant	[64]
K0	$1e^{-2}$	ruthenium redox constant	[64]
K01	$6e^0$	TPrA redox constant	[64]
Dru	$1e^{-9}[m^2/s]$	ruthenium diffusion coefficient	
Drup	$1e^{-9}[m^2/s]$	oxidized ruthenium diffusion coefficient	
Dtpa	$1e^{-9}[m^2/s]$	TPrA diffusion coefficient	
Dtpap	$1e^{-9}[m^2/s]$	oxidized TPrA diffusion coefficient	
Dpl	$1e^{-9}[m^2/s]$	byproduct diffusion coefficient	
Drue	$1e^{-9}[m^2/s]$	excited ruthenium diffusion coefficient	
L	$6 \times \sqrt{fracDru \times 2 \times abs(Emin - Emax)v}$	diffusion layer length	
K1	$K0 \times Dru/re$	ruthenium redox rate constant	
K2	$K01 \times Dtpa/re$	TPrA redox rate constant	
Eref_ru	$A \times log(c\_ru/c\_ref)$	ruthenium reference potential	
Eref_tpa	$A \times log(c\_tpa/c\_ref)$	TPrA reference potential	
c_ref	$1[mol/m^3]$	reference concentration that forces the TPrA equilibrium potential to be zero.	

Definitions

The "Definitions" node is a default node right under the "Model" node. In the present model, the "Definitions" node was used to define the variables os the model and an integration. Both can be reached by right-click on the "Definitions" node and selecting "variable" and "integration", the last one present on the "Model Coupling" sub menu.

The integration of the produced model in a spatial integration concerning the whole domain of the electrochemical cell. This operation is necessary in order to obtain a current density on the appropriate unit, since the current density calculated by the software is in $[A/m^2]$ and the desired unit is $[A/m]$. On the model, this operation is called by the command-line "intop1".
Variable is any parameter that is not generated automatically by the software and the user wants to observe. In the case of this work, the following variables were defined:

1. current. Defined as "intop1(elan.itotavg_els1)". This represents the spatial integration of the automatic generated electric current density(elan.itotavg_els1);

2. ECL. Defined as "$intop1(Kr \times rup * tpap - Ke \times rue)$". This represents the ECL signal generated by the cell and it is the spatial integration of the rate equation for the decay of the excited state ruthenium into the normal stable specie[63].

This are the only two phenomenons that this model is concerned that the graphics are not automatically generated by the software studies.

Geometry

The geometry of this model consists in an one dimension straight line, with the same length as the diffusion layer of the initial species (ruthenium and TPrA). This is enough to produce reliable results because the only mass transportation phenomena operating in the ECL cell is diffusion. Hence, all the reactions will occur on within the part of the electrolyte that is covered by the diffusion layer. The diffusion layer is computed by Equation 5.1.

5.4.2 Electroanalysis Node

After the backbone of the model is complete, the physics must be arranged. In the case of this work, "Electroanalysis (elan)" was selected from the "electrochemistry" branch. This physic defines the equations and boundary conditions that will be solved by the software. Every physics offers several nodes that will refine the boundary conditions of the system, in order to produce the most real result as possible. The nodes and boundary conditions definition fot the model of this work will be explained in the next sections.

In this node, the whole cell domain must be included. Also, the only mass transport mechanism considered is diffusion, hence the boxes of convection and electro-migration must be checked out.

On the "Dependent Variables" menu of this node, the number of chemical species that will, at some point, be present in the cell are defined. For this model, six species were defined and are listed below.

1. ru. Represents the $Ru(bpy)_3^{2+}$;
2. rup. Represents the oxidized state of $Ru(bpy)_3^{2+}$;
3. tpa. Represents the TPrA;
4. tpap. Represents the oxidized state of TPrA ;
5. rue. Represents the excited state of $Ru(bpy)_3^{2+}$;
6. p1. Represents the reaction byproduct.

Diffusion 1

This node is default. It will correspond to the domain selected on the "elan" physics unless it is overridden by another node. On this node, the diffusion coefficients of all species that will be used by the model. COMSOL set a standard value of 1^{-9} to all diffusion coefficients. In order to make this model more friendly to future users, the diffusion coefficients were defined on the parameters despite of the fact that they are the standard ones, so, when they need to be replaced, one must only modify the parameters table.

No Flux 1

This node is default. It will correspond to the domain selected on the "elan" physics unless it is overridden by another node. Since the model of this work does not consider any kind of electrolyte flux, no modifications need to be done in this node.

Initial Values 1

This node is default. It will correspond to the domain selected on the "elan" physics unless it is overridden by another node. In this physics, the initial values corresponds to the initial concentration of the chemical species of the cell. Since just the TPrA and the ruthenium are present in the beginning of the reaction, just their field must be filled with the corresponding parameter to their initial concentration. The other species are not present in the beginning of the study, so their fields are kept with zero. Figure 5.4.2 illustrates how the node should looks like after this step is completed.

Concentration 1

In this node the concentration on the boundary of the cell is defined. In the case of the model presented in this work, the extreme right boundary (boundary 2 in the geometry) is selected. The node is feeded with the same values as the "Initial Values 1". This because the solution can be defined as quiescent. Which means that the initial concentration is the same at any point of the cell.

Electrode Surface 1

This node defines what happens in the electrode/electrolyte interface. The first thing to be done here is to select a boundary that will represent the electrode. In the model of this work it will be the extreme left boundary of the geometry (boundary 1 in the geometry). After, the cyclic voltammetry test must be imposed. Hence, on the menu "Boundary condition" of the node, one must select "Cyclic Voltammetry". Once this is done, the software asks for definitions on the impulse applied to the electrode, such as the number of cycles, maximum and minimum potential and scan rate. After proper defining this parameters, the node should looks like Figure 5.4.2.

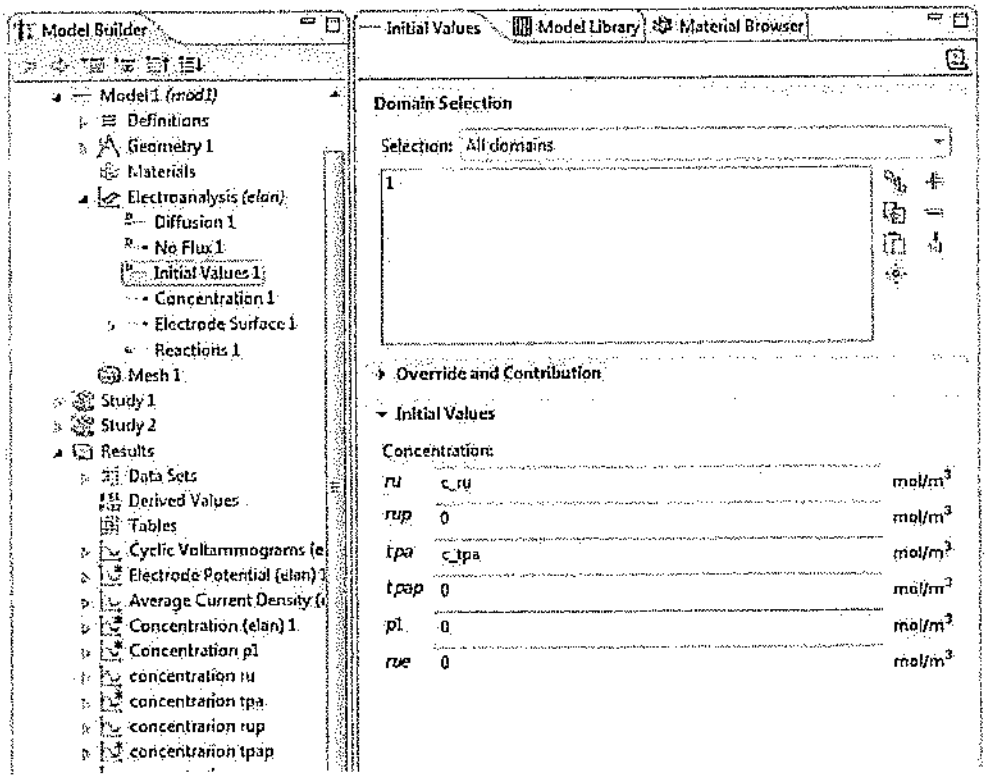

Figure 5.1: Initial Values node

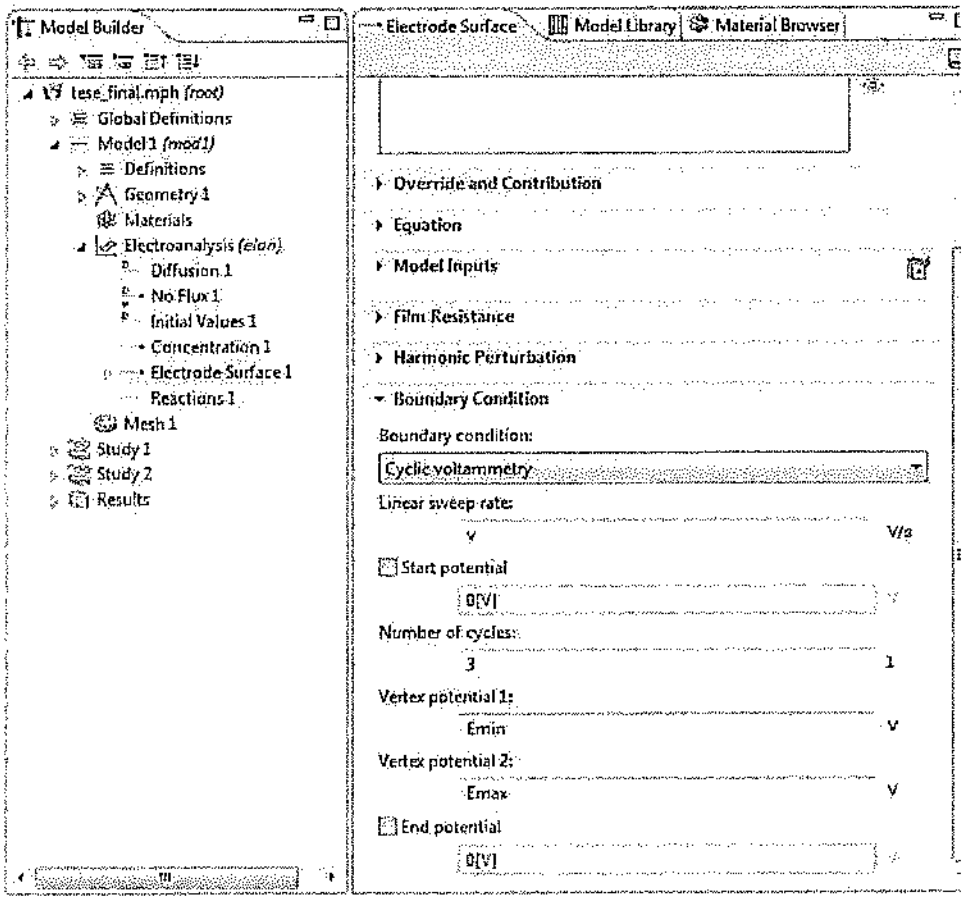

Figure 5.2: Electrode Surface node

After the proper definition of this node, the potential wave present on Figure 5.3 must be the input potential on the electrode.

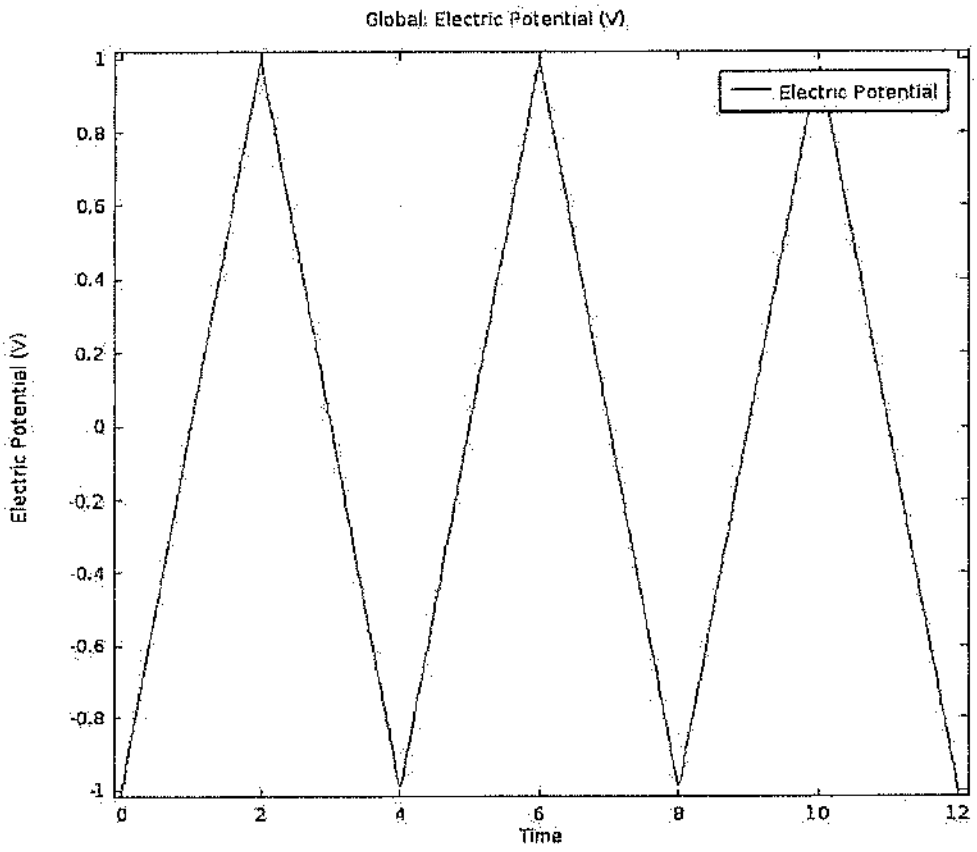

Figure 5.3: Applied potential

With a right click on this node, two "Electrode Reaction" sub-nodes are added, since two species are passing through redox equations (ruthenium and TPrA). On each one of these sub-nodes, the respective equilibrium potential for the reaction is added on the menu "Equilibrium potential at reference temperature". The "Electroanalytica Butler-Volmer" kinetics is selected for both redox processes, so the current will be dependent on the concentration of the chemical species. After that, the proper reaction rate constant is selected for each reaction from Table 5.4.1; the number of electrons participating on each reaction is defined, one electron for both reactions in the case of this model; and finally the stoichiometric coefficient of the reaction are defined, note that COMSOL assume the equation as a reduction, so the initial specie

has a stoichiometric coefficient of 1 and the oxidized specie a stoichiometric coefficient of −1. Figure 5.4 illustrates one of the two "Electrode Reaction" nodes after being proper defined for this model.

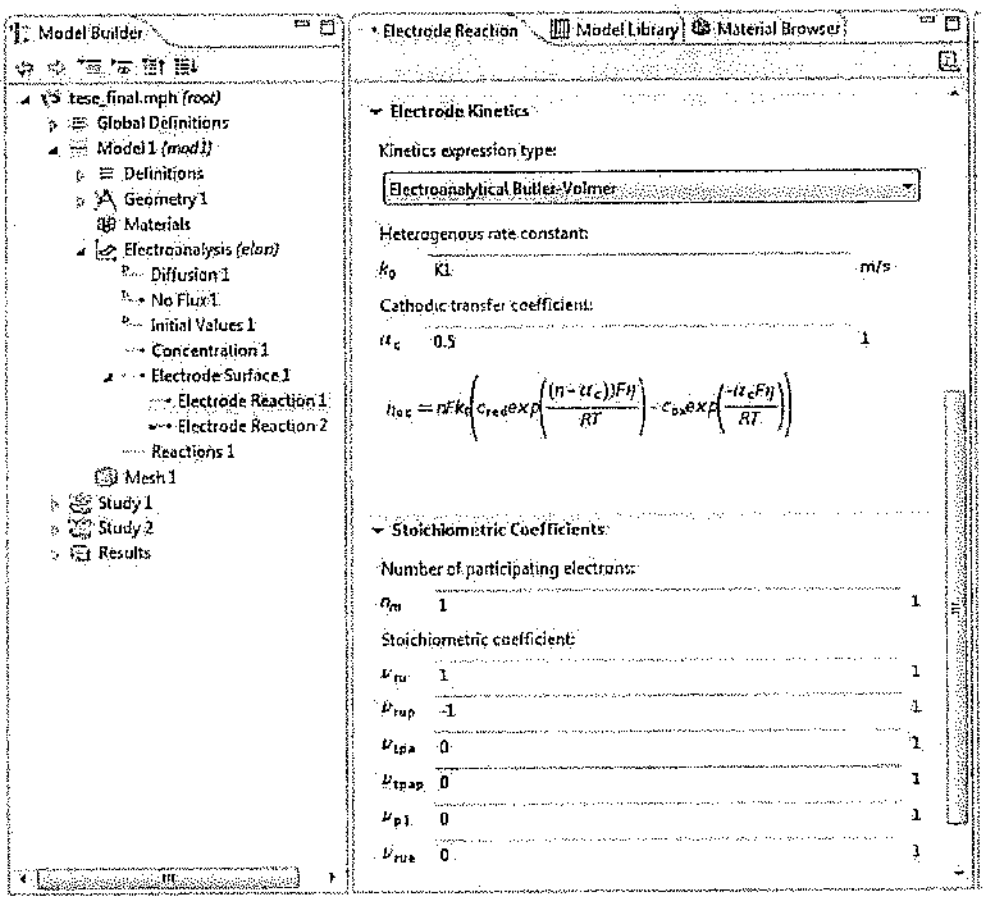

Figure 5.4: Electrode Reaction node for the ruthenium oxidation

Reactions 1

This node defines the chemical reactions that will happen inside the ECL cell based on the reaction rate of each chemical specie. The used reaction rates for this model were the standard ones from basic chemical equilibrium and consists of the rate constant for each reaction multiplied by the concentration of the reactants of the reaction. The unit of the rate constant is arbitrary, designed in a way that, when multiplied by all the concentrations

of the reactant, the final unit will be $[mol/(m^3 \times s)]$. When the reaction rate is positive, the specie is being produced in the system, when it is negative, the specie is being consumed by the system. The reaction rates for this model are shown on Figure 5.5.

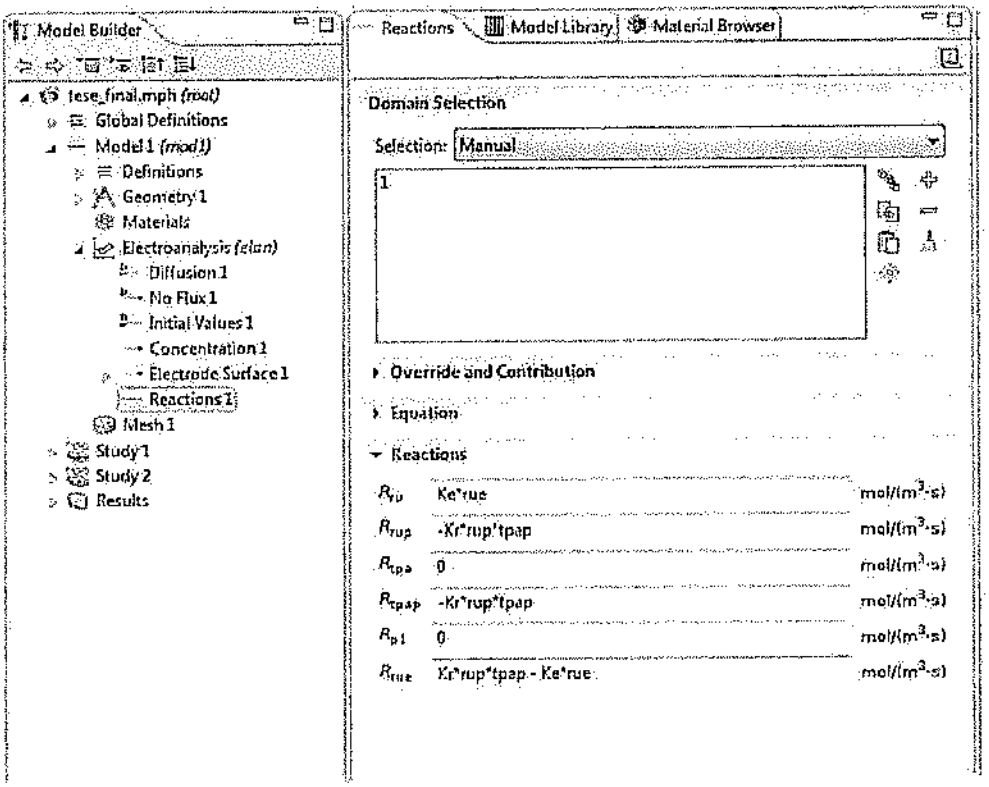

Figure 5.5: Reactions node

With this definitions, the model is considering the set of reactions represented on Equations 5.12 and 5.13. These equations are equivalent to the main reaction of the ruthenium/TPrA system.

$$rup + tpap \longrightarrow rue + p1 \tag{5.12}$$

$$rue \longrightarrow ru \tag{5.13}$$

5.4.3 Studies

The final step on constructing the model is defining the studies. For this model, two studies will be used. They are described inn the following sections.

Cyclic Voltammetry

This study performs a cyclic voltammetry on the defined system. It will generate, automatically, the cycli voltammogram and a graphic with the current density. For the model present in this work, no modifications need to be made in this node.

Time Dependent

This study will be used to observe the behavior with respect to time of the concentration of the chemical species present in the ECL cell. The observed time interval must be wide enough to contain all voltammetric cycles of the CV study.

5.4.4 Model Build

To build this model from the beginning on COMSOL, when open a new model on the software, first the dimension of the model must be selected, in this case, one dimension; after, the physics must be selected, for this model, one must open the "Electrochemistry" branch and select the "Electroanalysis" physics; finally, the "cyclic voltammetry study" is selected and the model root is generated. Since two studies are needed, right-click on the model root to and another study, in this case, "Time dependent".

5.5 Results

The results of this model are the cyclic voltammogram and the evolution in time of the current density and the concentrations of the species present in the ECL cell. Each of these are discussed in the following sections.

5.5.1 Cyclic Voltammogram

The cyclic voltammogram is a graphic of the current density flowing through the system with respect to the applied potential, defined on section "COMSOL Implementation". Can be observed on Figure 5.6 that the voltammogram of the modeled system has two pairs of peaks, one for the TPrA oxidation/reduction and othe for the ruthenium oxidation/reduction. The TPrA peaks are the most prominent ones and the appear on lower voltages. The position of the peaks depends on the number of electrons involved in the redox process and on the constant rate of the redox reactions. Hence, the TPrA peaks happen much closer to zero because the rate constant for the redox process is far bigger than the rate constant for the ruthenium redox process. The influence in the magnitude depends on the concentration of the specie in the cell. Since the initial concentration of TPrA is also bigger than the initial concentration of ruthenium, it is the main responsible for the current generation. Due to this fact, the ruthenium peaks are much smaller and difficult to be localized in this type o graphic.

An important feature to highlight is that the ECL signal is emitted most brightly on the time correspondent to the ruthenium peaks. So the model predict the light emission on the time where the potential reaches, approximately, $0.58V$ (positive peak) and $-0.62V$ (negative peak). The ruthenium peaks are not symmetric with respect to zero potential due to the equilibrium potential, slightly negative in the case of this setup.

5.5.2 Current Density

Figure 5.7 presents the evolution of the current density with respect to time. Two important features must be observed in this graphic. The first is the decay of the maximum value for every cycle caused by the consumption of the TPrA in the process. The TPrA is not regenerated by the system and so the maximum of the first cycle cannot be reached again. The same decay is expected to be observed in the TPrA concentration graphic and on the ECL signal graphic. The second thing to be observed is that the maximum of current is coincident with the TPrA peak con the cyclic voltammogram. The normal decrement on the current value is interrupted bu a very small secondary peak between 1 and 2 seconds. This peak is due to the ruthenium peak of the cyclic voltammogram. In the case of the studied system, is easier to localize the ruthenium peak in the current density graphic than in the cycli voltammogram itself. Since the two peaks are coincident, the ECL

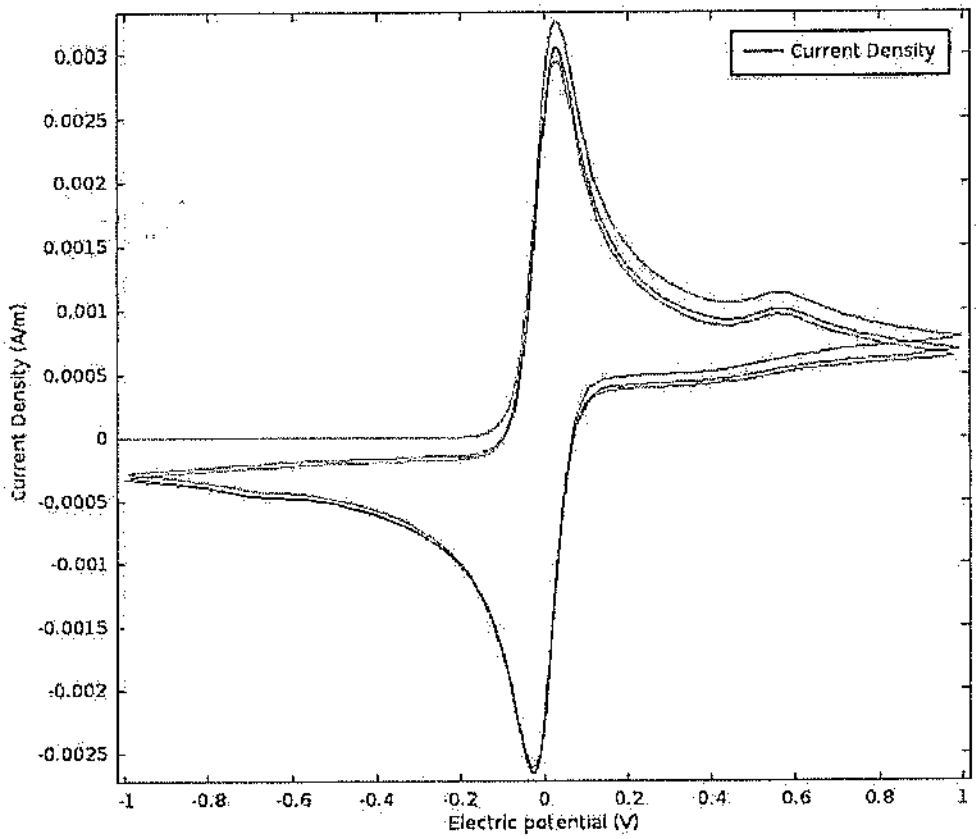

Figure 5.6: Cyclic voltammogram for the ruthenium/TPrA system

signal emission can also be predicted by the position of the secondary peak on the current density graphic, and it is expected to happen, for the positive part of the first cycle, between 1 and 2 seconds from the beginning of the test.

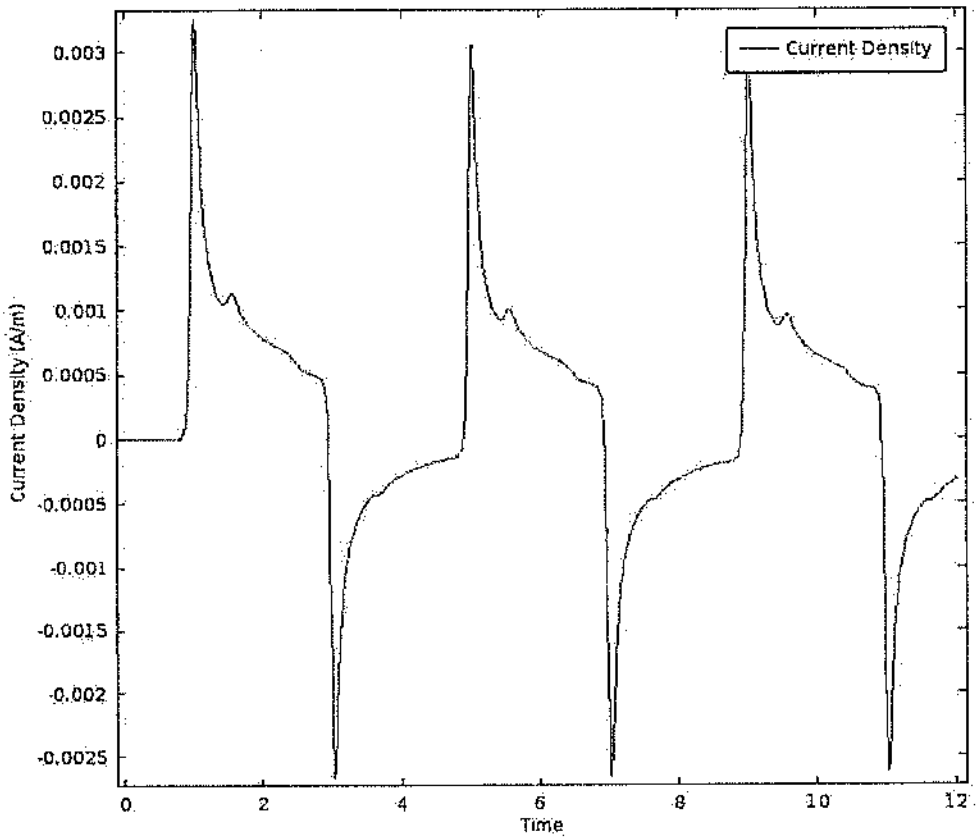

Figure 5.7: Current density

5.5.3 Ruthenium Concentration

Figures 5.8, 5.9 and 5.10 presents the evolution on time of the concentrations of ruthenium, oxidized ruthenium and excited ruthenium, respectively. Since the ruthenium is regenerated by the system, the maximum values of Figures 5.8 and 5.9 are constant over the cycles, also important to notice these two figures are complementary. The same regenerative behavior is not observed in the excited ruthenium 5.10 because this form is generated in a reaction involving TPrA (Equation 5.10) that is being consumed and

transformed into by products. As a consequence, the magnitude decay observed here has the same behavior observed in the current density graphic. And, since the ECL signal depends on the excited ruthenium concentration(Equation 5.11), this graphic alone demonstrates the correctiveness of the model with respect to the loss of signal intensity over the voltage cycles, observed experimentally.

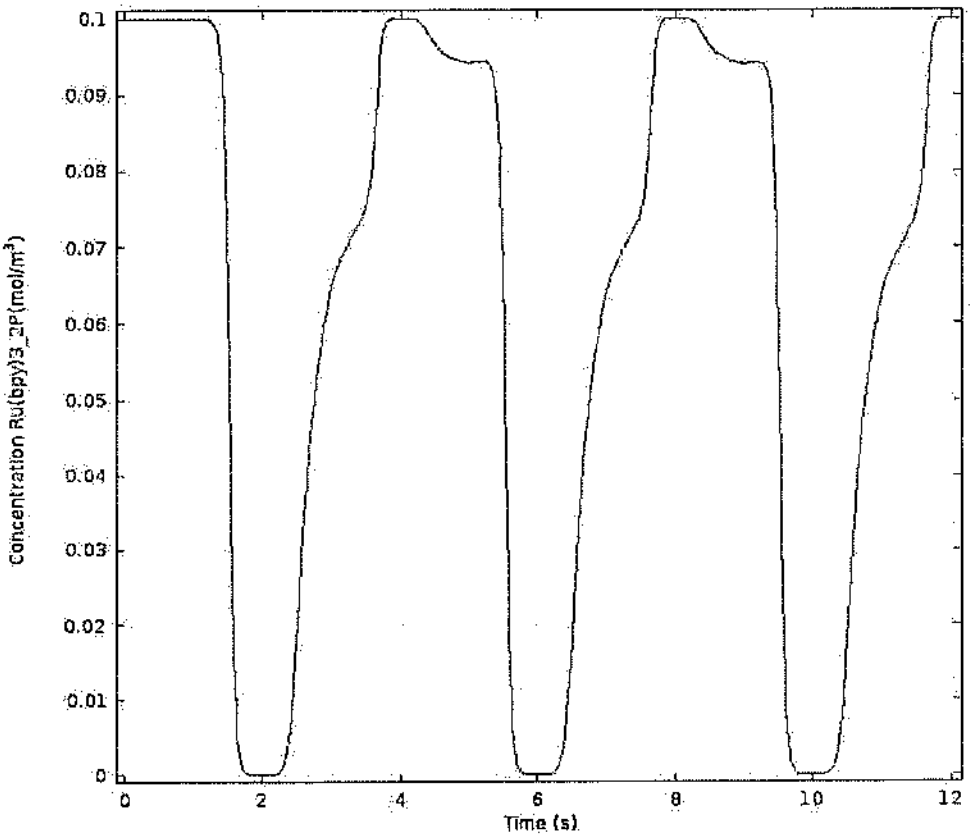

Figure 5.8: Concentration of the Ruthenium

5.5.4 TPrA Concentration

Figures 5.11 and 5.12 present the evolution of the concentrations of TPrA and oxidized TPrA, respectively, over time. Again, these two graphics are complementary and the decay of the maximum value over the cycles is due to the consumption of the specie by the system reactions. The envelope that

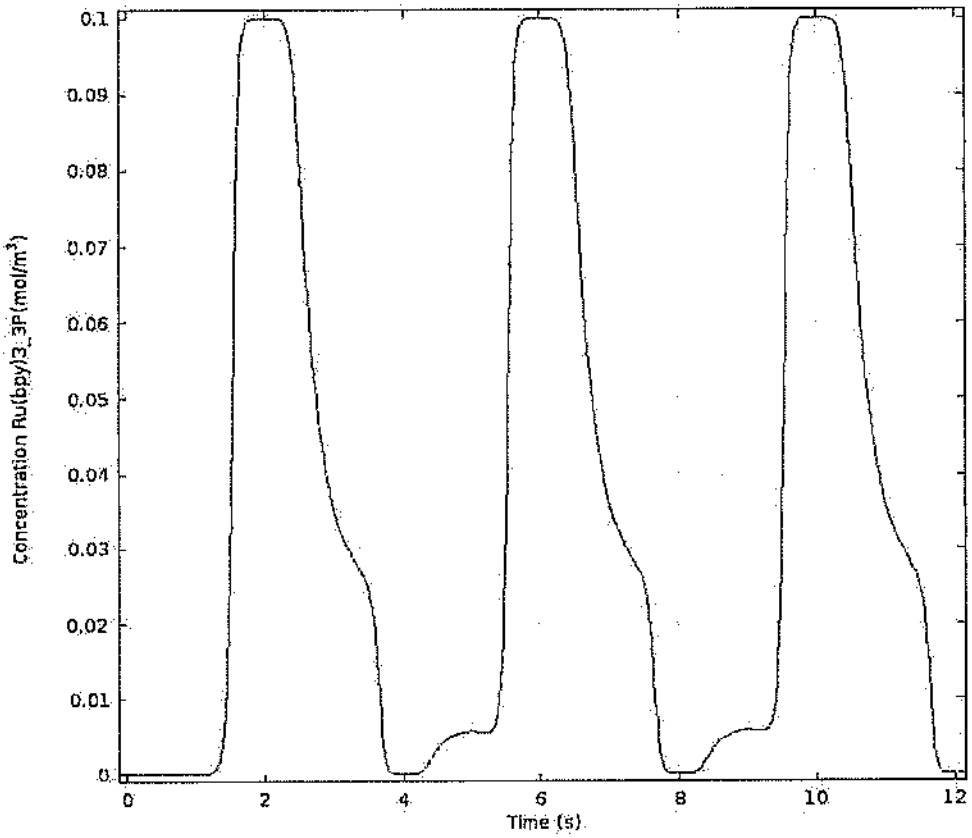

Figure 5.9: Concentration of the oxidized ruthenium

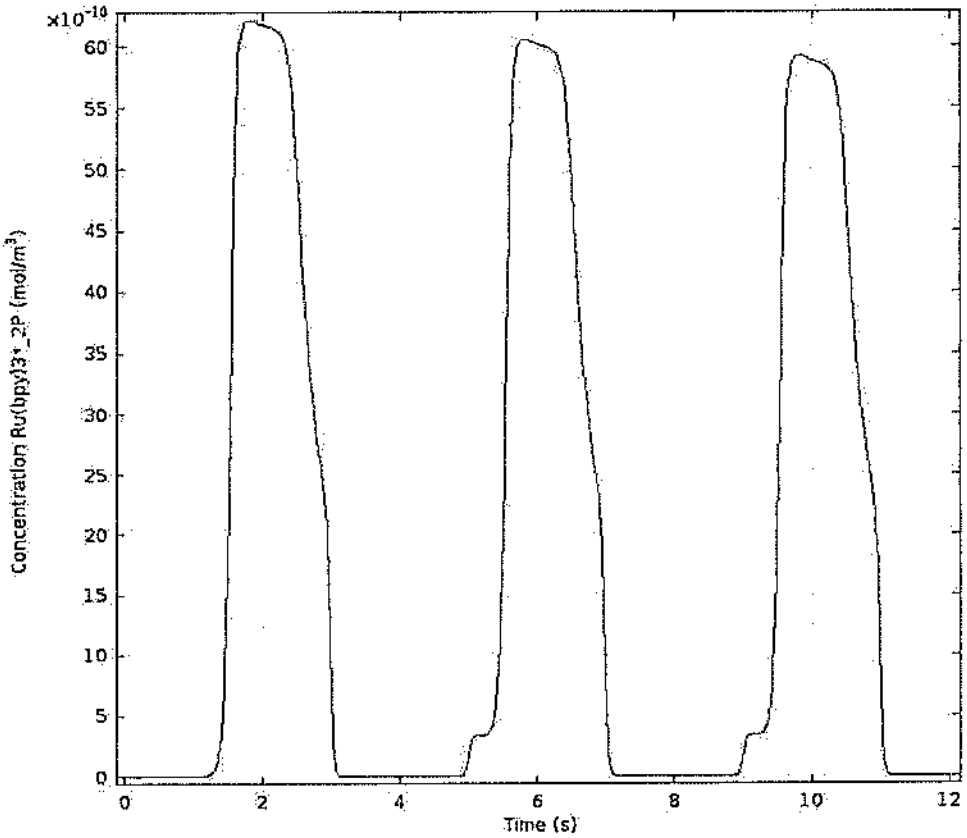

Figure 5.10: Concentration of the excited ruthenium

covers the decay is the same one observed on Figures 5.7 and 5.10.

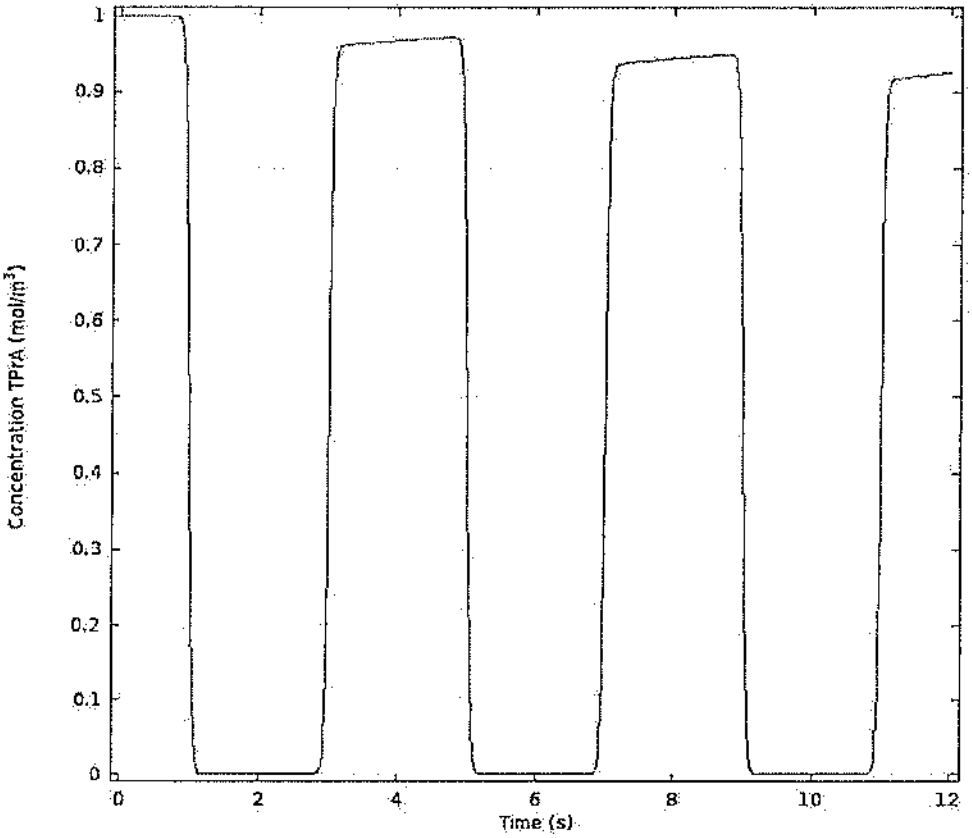

Figure 5.11: Concentration of the oxidized ruthenium

5.5.5 ECL Signal

Figure 5.13 presents the evolution of the ECL signal over time. It can be observed that the maximum of the light emission is coincident with the secondary peaks on Figures 5.6 and 5.7, and also that the intensity decrement for every passed cycle. The unique features of this graphic are the observation of light emission on the negative part of the voltage cycle and that the maximum values for the negative part are smaller than the positive peaks. Also, the negative peaks do not present any intensity decrement over the cycles. This is because the limiting factor for the emission in the positive part of the cycle is the concentration of TPrA, while for the negative part the

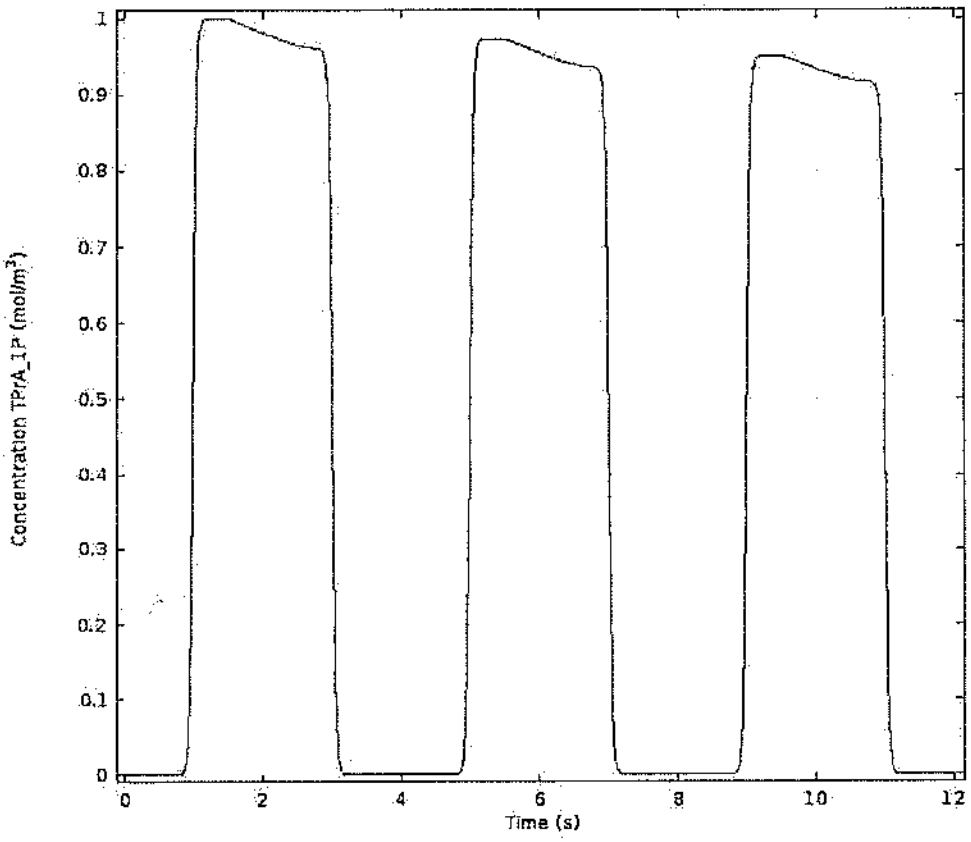

Figure 5.12: Concentration of the oxidized TPrA

emission is limited by other factors. Is expected that, for more voltammetric cycles, the peaks negative part also start to decay when the intensity of the peaks on the positive part reaches the same intensity value.

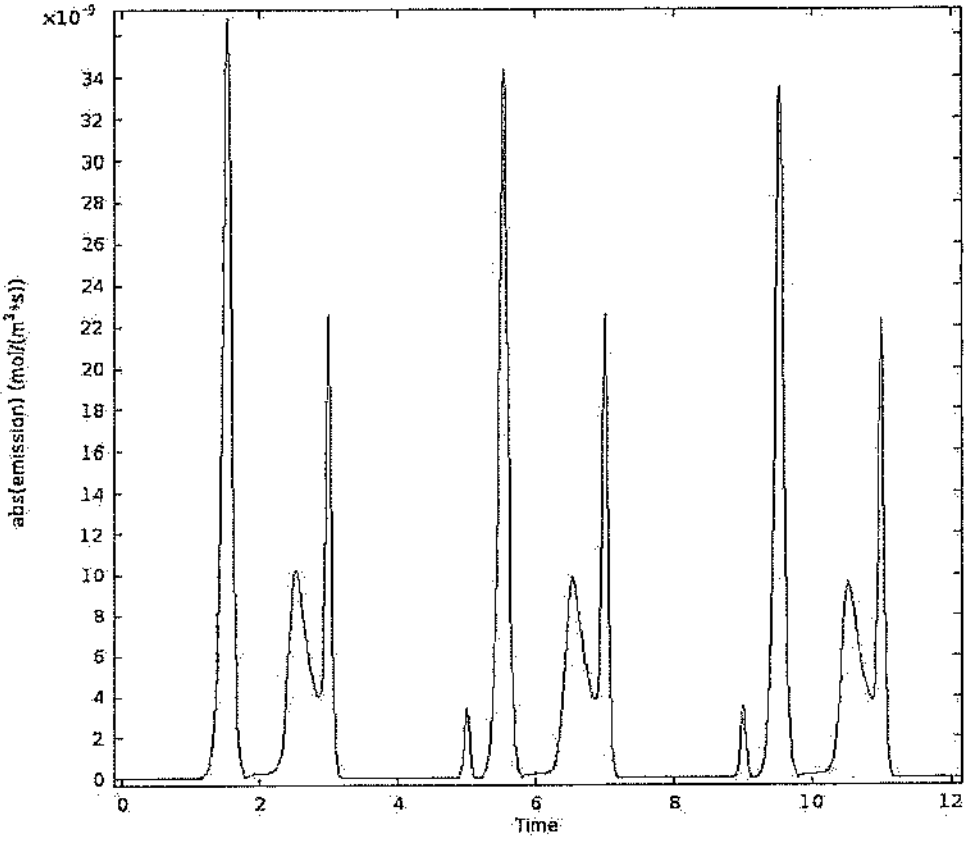

Figure 5.13: ECL signal

5.6 Possible Improvements

This model is effective in providing a first approximation for the studied phenomena. To improve the model precision, the following features can be included:

1. Include the side reactions of the ruthenium/TPrA system. This can be

done by adding the chemical species present on the side reactions and de

ning their rate expression on the reactions node. In this operation, one must be careful with the convergence of the model, since big differences in the absolute values of the rate expressions can compromise the model convergence.

2. Include the dependency on the pH. The pH is can be de

   ned as a measurement of the H^+ concentration. So this concentration must be de

   ned, also the loss of protons by the oxidized TPrA must be defined as a reversible reaction. This two modi

   cations will, probably, simulate the decrease of the ECL signal for lower pH.

3. Include the electrolyte ohmic resistance.

4. Apply proper values for the diffusion coefficients of the chemical species.

5. Expand the dimension of the model.

6. Introduce the effect of water electrolysis on the system.

5.7 Secondary reactions

In this section, the secondary reactions of the Ruthenium/TPrA system were included in the model. Which will, hopefully, increase the precision of the simulated results and present new aspects to the software output, providing a better approximation to real experiments.

This section will first present the reactions that were included, then it will explain the modifications made on the software and finally present the results of the modified model, with a brief comparison with the results on the previous section.

5.7.1 Boundary Conditions

Though the mechanism of the Ruthenium/TPrA system was exaplained in details on chapter 3, the reactions that were included on this new version

of the model are repeted below. They contribute with two new cycles of luminescense.

First cycle:

$$Ru(bpy)_3^{2+} + TPrA^{\bullet} \longrightarrow Ru(bpy)_3^{+} + P1 \tag{5.14}$$

$$Ru(bpy)_3^{+} + Ru(bpy)_3^{3+} \longrightarrow Ru(bpy)_3^{2+*} + Ru(bpy)_3^{2+} \tag{5.15}$$

Second cycle:

$$TPrA^{\bullet+} + Ru(bpy)_3^{+} \longrightarrow Ru(bpy)_3^{2+*} + TPrA \tag{5.16}$$

These new cycles require the inclusion of one new chemical specie in the software, which is $Ru(bpy)_3^{+}$ (represented by "run"). All the other species are already present in the previous version of the model.

Also, there is no new equation that must be solved, the update consists only in considering these two new sets of equations and observing how they influence the system behavior.

5.7.2 COMSOL Implementation

Parameters

In order to include the new sets of reactions, the rate constante of the reactions between $Ru(bpy)_3^{+}$ and $Ru(bpy)_3^{3+}$, and $TPrA^{\bullet+}$ and $Ru(bpy)_3^{+}$ were included on the parameters table as Kr3 and Kr4, respectively. The values were again stracted from R. Mark Wightman work [?].

Electroanalysis Node

This is the node where we add the new chemical specie "rup". Also, the side reactions introduced many disturbes in the system. As a consequence, more voltage cycles had to be introduced, so the system could pass the transient phase and we were able to observe the stationary behavior. In his simulation, 15 cycles were used in the CV test.

Reactions1

In this node, all reactins rates had to be rewrited due to the presence of the side reactions, this is because they influence the concentration of the chemical species that where present on the main reaction. Figure 5.14 presents a printscreen of the reaction node used in this simulation, where all reaction rates are written in function of the concentration of the respective reaction products and rate constant.

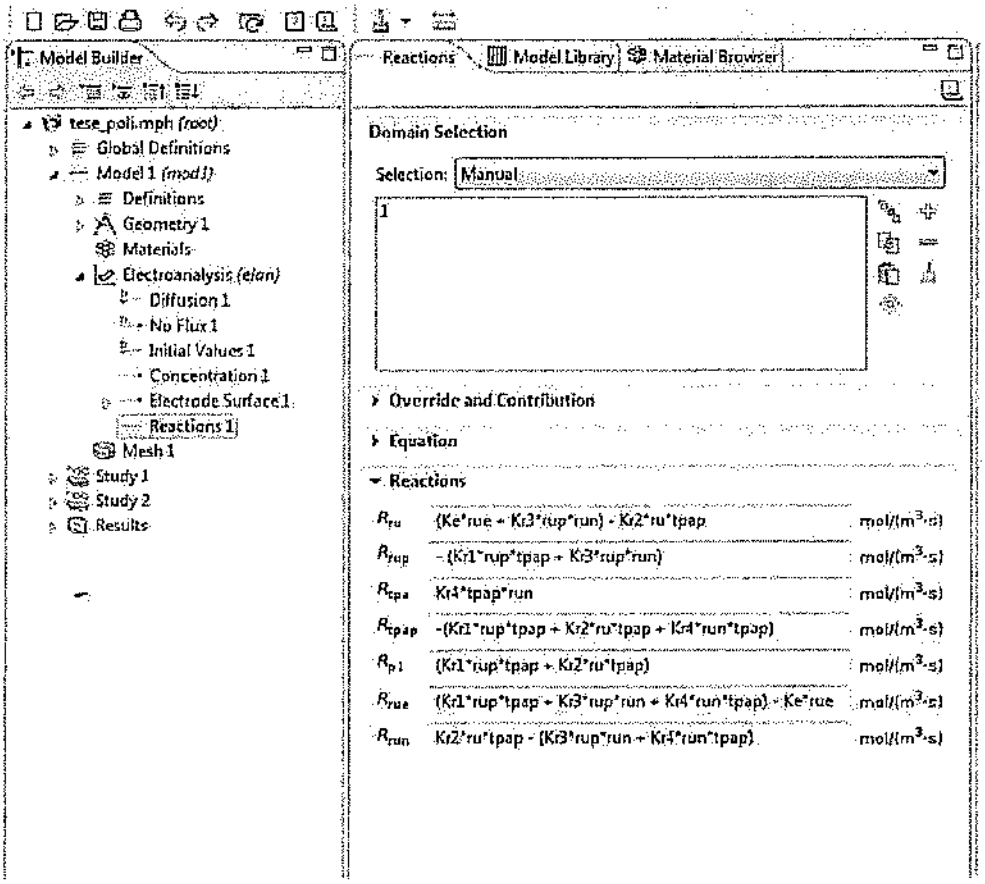

Figure 5.14: Reactions node updated

5.7.3 Updated Results

This subsection presents the results of the simulation of the updated software. The main goal is to stablish a comparison between these results with

the ones presut on section 5.5. For a more detailed explanation about the importance of each graphic, is recomended to consult section 5.5.

Cyclic Voltammogram

The cyclic voltammograms of the two models present in this work are very similar. In fact, the main difference is that the cyclic voltammogram of the model with the side reactions have more cycles. These extra cycles were included in order to overcome the transiient that will be present in the next graphics.

This similarity is, in fact, expected, because though more reactions are happening inside the electrolytic cell, nothing was alterated in the electro/electrolyte interface, which is the place that most influence the cyclic voltammogram.

5.7.4 Current Density

Figure 5.16 presents the current density with respect to time of the updated model. Again, the current density of the two models are very alike. Both presents the exponential decay and the secondary peaks. Again, this is expected because the region that is being analysed by this graphic is the interface between the electrode and the electrolyte.

Ruthenium Concentration

Figures 5.17 to 5.20 present the evolution of the concentration of $Ru(bpy)_3^{2+}$, $Ru(bpy)_3^{3+}$, $Ru(bpy)_3^{2+*}$, respectively.
Now, substantial differences between the two models can be observed. Initially, in the model without the side reactions, all $Ru(bpy)_3^{2+}$ were regenerated, so its concentration was equal to its initial concentration in the begining of every cycle. When the side reactions are included, a huge concentration drop is observed between the first and the second cycle. After that, the concentration starts to varry its value until it stabilizes on 0.062 mol/L close to the fifth cycle. this means that there is a considerable amount of ruthenium, 38% of the initial concentration, that remains on other oxidation state, more specifically, in the $Ru(bpy)_3^+$ form, as shown on Figure 5.19. As a result, the concentration of $Ru(bpy)_3^{3+}$, Figure 5.18, is also smaller when compared with

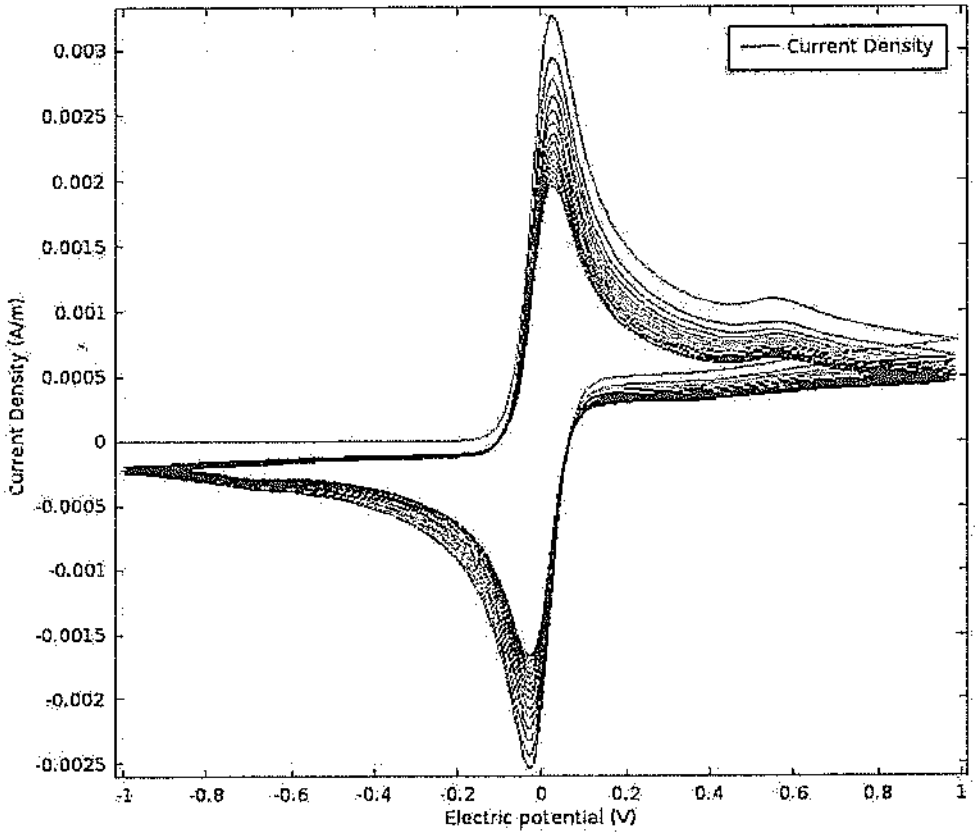

Figure 5.15: Cyclic voltammogram for the ruthenium/TPrA system updated

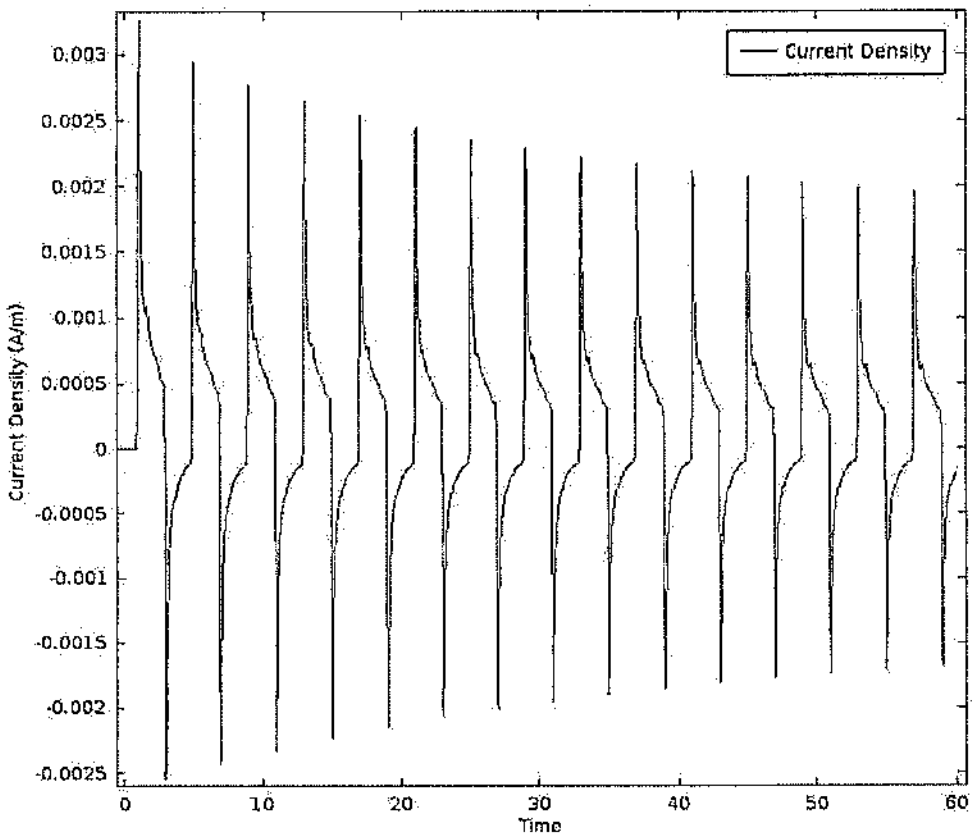

Figure 5.16: Current density updated

the model without the side reactions.

The concentration of $Ru(bpy)_3^{2++}$ is a bit more delicate to be analyzed because all reactions contribute to its generation. When compared wiht Figure 5.10, Figure 5.20 presents a similar maximum of $6210^{-10} mol/m^3$, but a much faster decay. Since the amount of photons liberated by the process depends on the concentration of molecules on the excited state, a similar behavior is expected on the ECL signal.

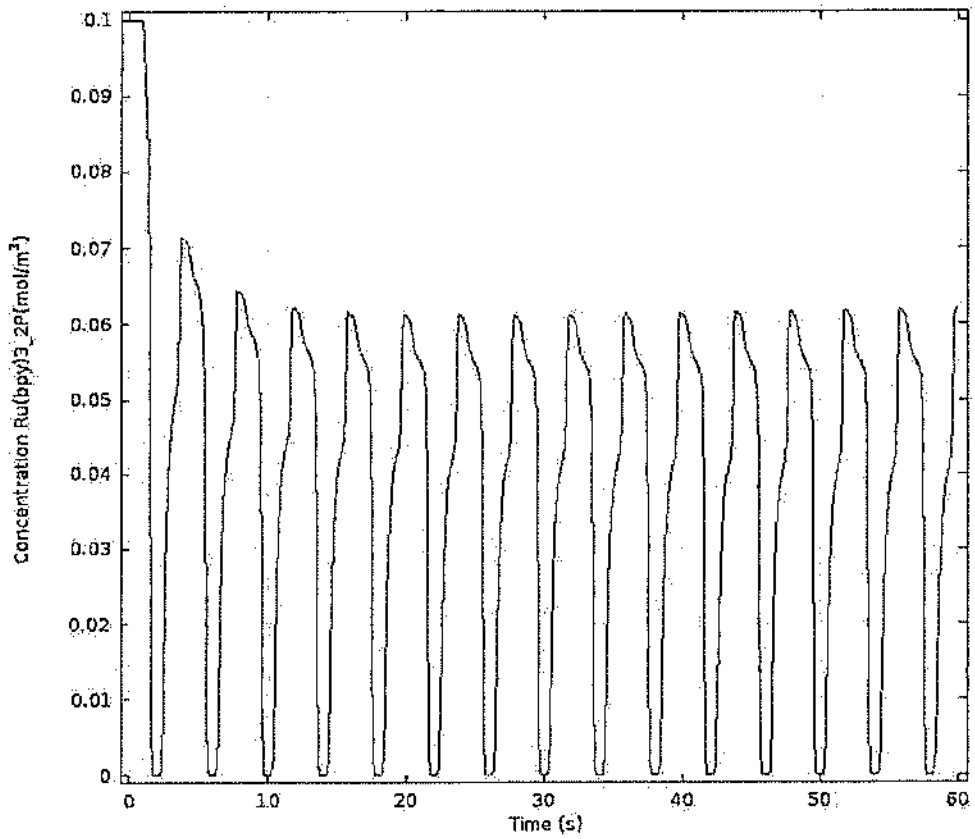

Figure 5.17: Concentration of the Ruthenium updated

TPrA Concentration

Despite of the fact that the TPrA is now being regenerated by Equation 5.16, the overall behavior fo its concentration still the same with respect

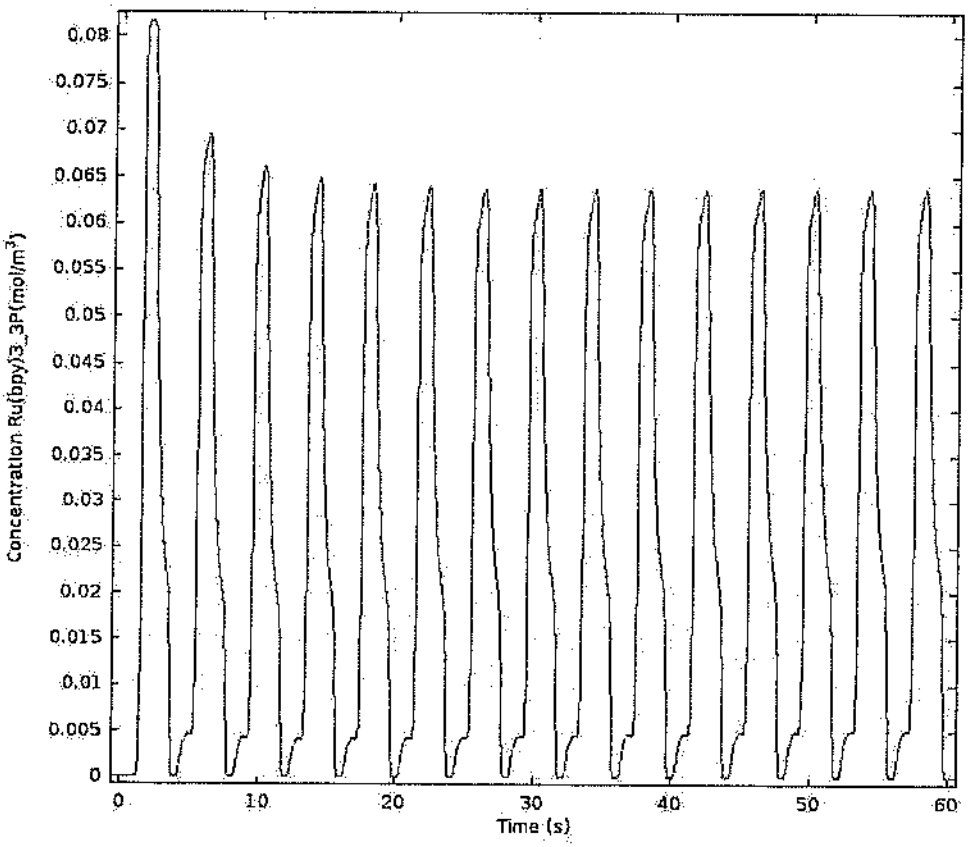

Figure 5.18: Concentration of the oxidized ruthenium updated

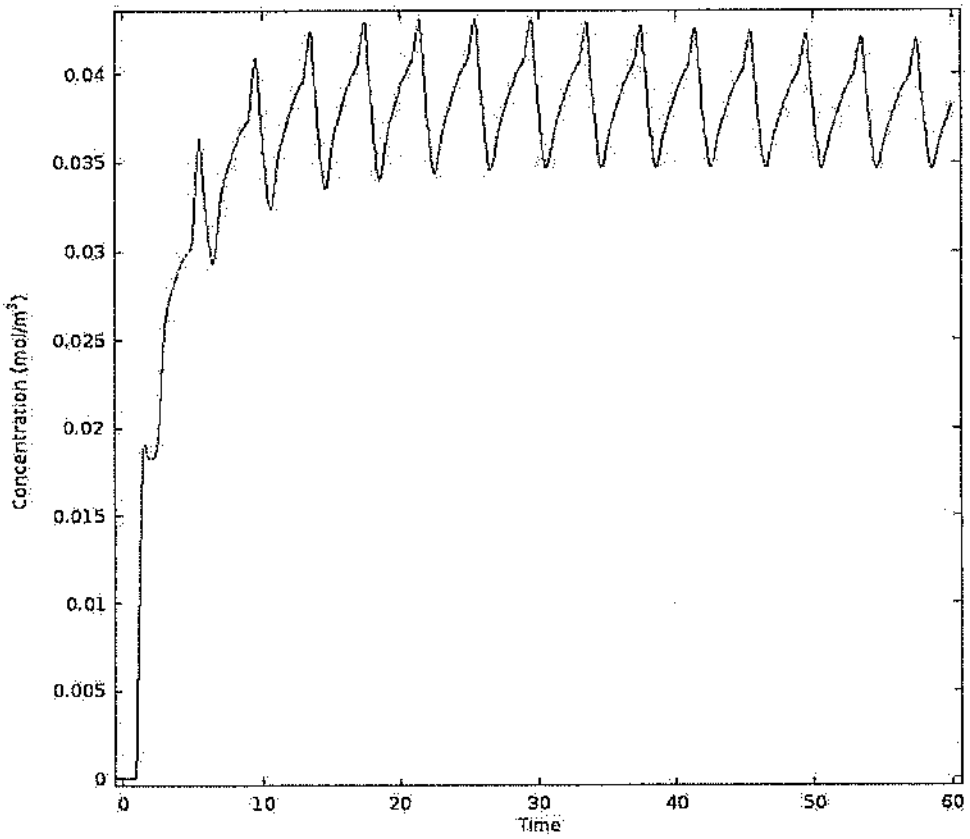

Figure 5.19: Concentration of the oxidized ruthenium updated

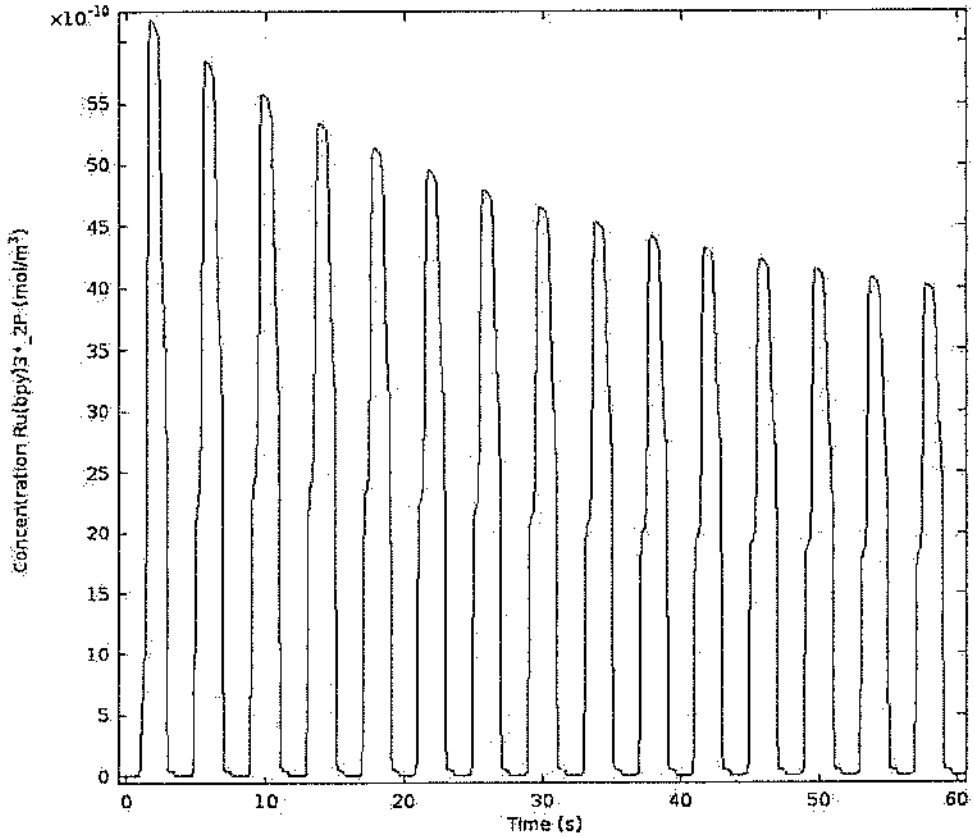

Figure 5.20: Concentration of the excited ruthenium updated

to the model without the side reactions. This is expected because the consumption of this specie is more common and faster than its regeneration, and also, it's being converted to a substance that is inert to the process. That means that after each cycle, there is less TPrA to be used and regenerated. The concentration of TPrA, $TPrA^{\cdot}$ and the inert substance are present on Figures 5.21, 5.22 and ??.

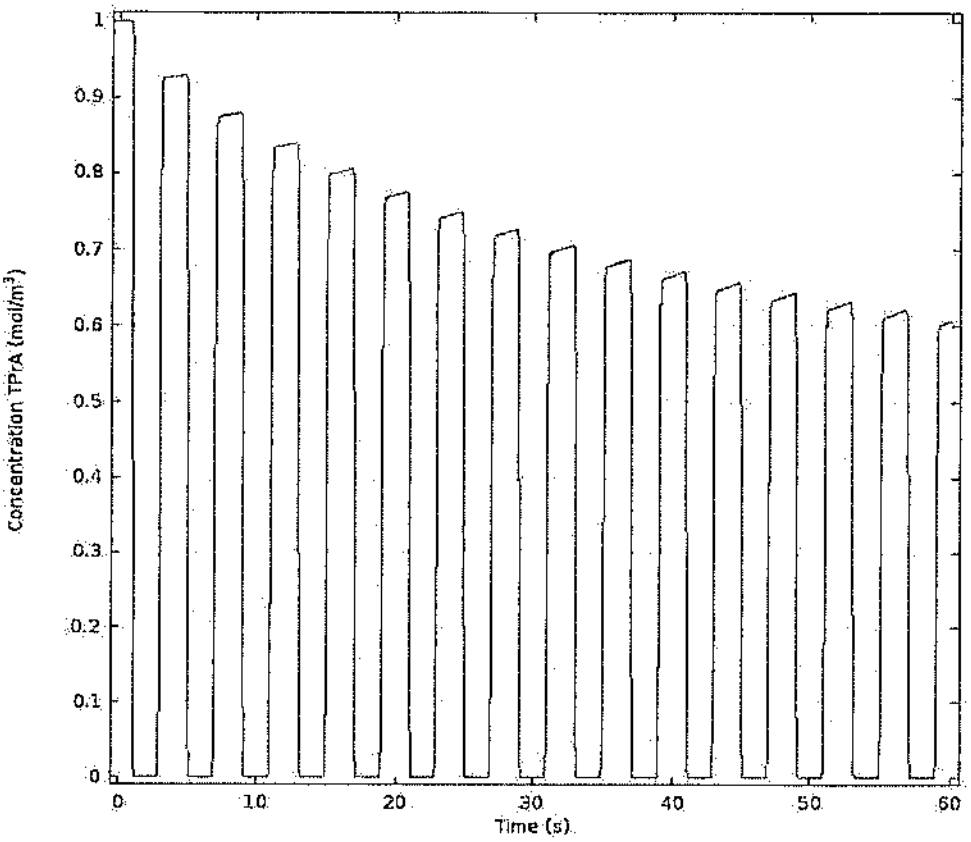

Figure 5.21: Concentration of the TPrA updated

ECL Signal

As expected, the maximum value of the signal, present in Figure 5.24, is smaller than in the simpler model. The time synchronization explained on section 5.5.5 of this work still present, but there is a third signal peak due to the side reactions that is know relevant. Also, it follows the behavior of

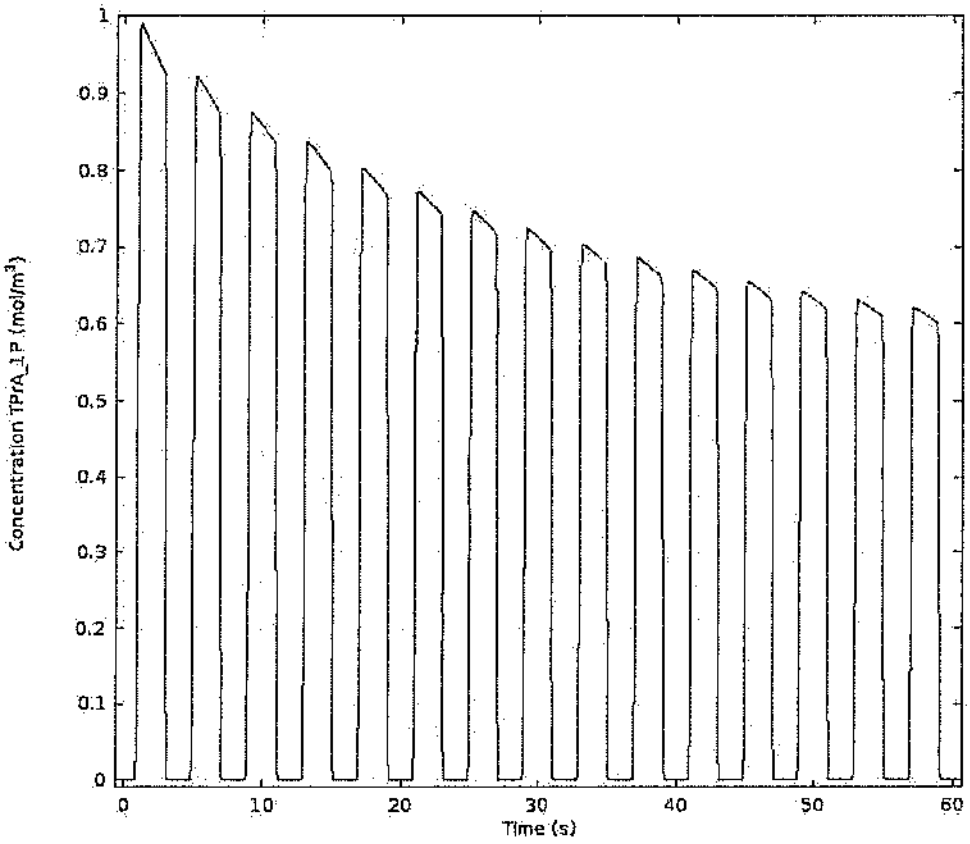

Figure 5.22: Concentration of the oxidized TPrA updated

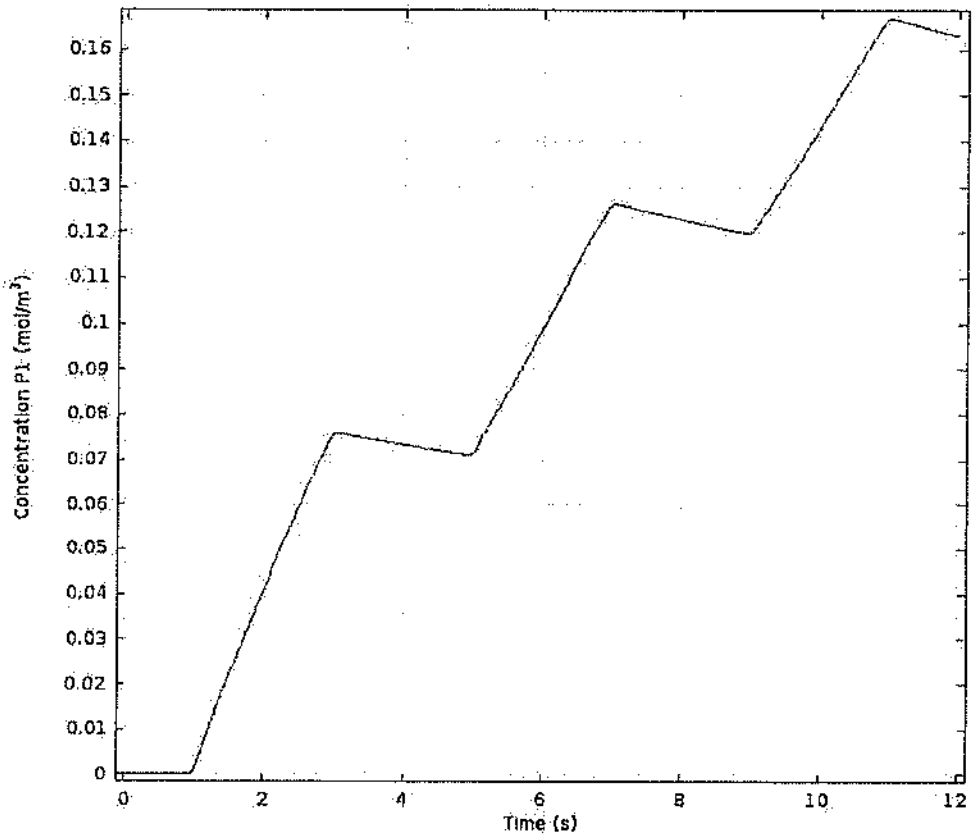

Figure 5.23: Concentration of the oxidized TPrA updated

the ruthenium concentration, with a very notable transient until the fifyth cycle, then stabilizing.

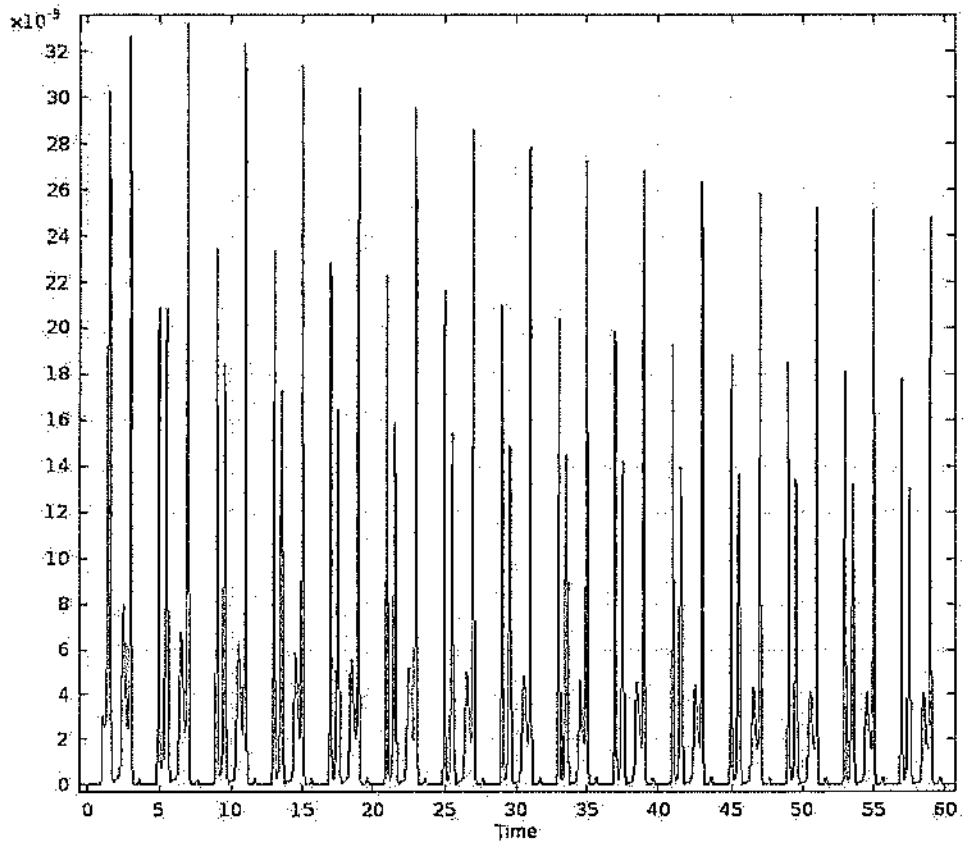

Figure 5.24: ECL signal updated

Chapter 6

Conclusion

This Master Thesis presents a COMSOL Mulriphysisc model for the cyclic voltammetry test on Ruthenium/TPrA ECL system. The model consists of an one dimension geometry and only takes into account the first reaction wave of the system, simplifications made to keep a low computational cost.

Despite of the simplifications, the model was able to predict the system behavior. The qualitative behavior of all graphics generated by the model were according to the experimental tests previously performed at the laboratory of Politecnico di Torino (MiNES), where I did my work. The main difference between the model output and the experimental data is the position of the secondary peaks on the cyclic voltammogram. Experimentally, these peaks appers close to $-0.8V$ and $0.8V$, while these same peaks were predicted to apper close to $-0.6V$ and $0.6V$. This difference implies that the model predicts the light emission before it actually happens on the experiment. This position difference is believed to be caused by the electrode radius, because while the experiments use a micro-electrode, the model is taking into account a macroscopic electrode.

This model can be improved by adding the second reaction wave of the ruthenium/TPrA system and the inclusion of the pH influence on the ECL signal. Expanding it to two or three dimensions is also possible, but it is a secondary feature, since most of the system dynamics occurs within the diffusion layer and it can be very well represented by the one dimension model. Another aim of this work was to build a model that can be easily learned and modified in future works. The way that the model was build satisfy that feature. To proceed studies with different electrode radius, initial concentrations or even potential waves, it is only necessary to perform the desirable modifications on the parameters table an the model will provide the results

for the new set-up. To perform deeper modifications, such as model another ECL system, the reading of Chapter 5 of this work is recommended. This chapter provides a quick tutorial on how to build the presented model, so by reading it, one can master the model and perform the desired tests.

As a complement to the work done at Politecnico di Torino, the side reactions were implemented on the model. This modification resulted in the appearence of a transient on the ECL signal, where the first voltametric cyclic is not the one with the strongest signal. Also, the process has lost effiency and presents a faster decay. Unfortunately, the results of the model cannot be compared with experiments, since there is no experiments concerning this system at Escola Politecnica de São Paulo. As a future complement to this work, we intent to study and implement experimentally this system at Poli Usp.

Bibliography

[1] Dufford, R. T.; Nightingale, D.; Gaddum, W. L. J. Am. Chem. Soc. 1927, 49, 1858.

[2] Harvey, N. J. Phys. Chem. 1929, 33, 1456.

[3] Hercules, D. M. Science. 1964, 145, 808.

[4] Rubinstein, I.; Bard, A. J. Am. Chem. Soc. 1981, 103, 512.

[5] C. G. Zoski, Handbook of Electrochemistry, 2007. [Online]. Available: http://www.sciencedirect.com/science/book/9780444519580

[6] F. E. Beideman and D. M. Hercules, Electrogenerated chemiluminescence from 9,10-diphenylanthracene cations reacting with radical anions, The Journal of Physical Chemistry, vol. 83, no. 17, pp. 22032209, 1979. [Online]. Available: http://pubs.acs.org/doi/abs/10.1021/j100480a005

[7] L. R. Faulkner, H. Tachikawa, and A. J. , Electrogenerated chemiluminescence. vii. influence of an external magnetic field on luminescence intensity, Journal of the American Chemical Society, vol. 94, no. 3, pp. 691699, 1972. [Online]. Available: http://pubs.acs.org/doi/abs/10.1021/ja00758a001

[8] Electrogenerated chemiluminescence. vii. influence of an external magnetic field on luminescence intensity, Journal of the American Chemical Society, vol. 94, no. 3, pp. 691699, 1972. [Online]. Available: http://pubs.acs.org/doi/abs/10.1021/ja00758a001

[9] A. Pighin and B. E. Conway, A correlation between the quantum efficiency of electrogenerated chemiluminescence and the redox potentials of rubrene in various solvents, Journal of The Electrochemical Society, vol. 122, no. 5, pp. 619624, 1975. [Online]. Available: http://jes.ecsdl.org/content/122/5/619.abstract

[10] T. C. Werner, J. Chang, and D. M. Hercules, Electrochemiluminescence of perylene. the role of direct exciner formation, Journal of the American Chemical Society, vol. 92, no. 19, pp. 55605565, 1970. [Online]. Available: http://pubs.acs.org/doi/abs/10.1021/ja00722a005

[11] J. T. Maloy and A. J. Bard, Electrogenerated chemiluminescence. vi. efficiency and mechanisms of 9,10-diphenylanthracene, rubrene, and pyrene systems at a rotating-ring-disk electrode, Journal of the American Chemical Society, vol. 93, no. 23, pp. 59685981, 1971. [Online]. Available: http://pubs.acs.org/doi/abs/10.1021/ja00752a004

[12] R. Y. Lai, J. J. Fleming, B. L. Merner, R. J. Vermeij, G. J. Bodwell, and A. J. Bard, Electrogenerated chemiluminescence. 74. photophysical, electrochemical, and electrogenerated chemiluminescent studies of selected nonplanar pyrenophanes, The Journal of Physical Chemistry A, vol. 108, no. 3, pp. 376383, 2004. [Online]. Available: http://pubs.acs.org/doi/abs/10.1021/jp0367981

[13] E. A. Chandross, J. W. Longworth, and R. E. Visco, Exciner formation and emission via the annihilation of electrogenerated aromatic hydrocarbon radical cations and anions, Journal of the American Chemical Society, vol. 87, no. 14, pp. 32593260, 1965. [Online]. Available: http://pubs.acs.org/doi/abs/10.1021/ja01092a054

[14] J. B. Ketter and R. M. Wightman, Tuning emissive states in electrogenerated chemiluminescence, Journal of the American Chemical Society, vol. 126, no. 32, pp. 10 18310 189, 2004, pMID: 15303894. [Online]. Available: http://pubs.acs.org/doi/abs/10.1021/ja047602t

[15] I. Rubinstein and A. J. Bard, Electrogenerated chemiluminescence. 37. aqueous ecl systems based on tris(2,2 bipyridine)ruthenium(2+) and oxalate or organic acids, Journal of the American Chemical Society, vol. 103, no. 3, pp. 512516, 1981. [Online]. Available: http://pubs.acs.org/doi/abs/10.1021/ja00393a006

[16] A. Bard and L. Faulkner, Electrochemical Methods: Fundamentals and Applications. John Wiley and Sons, 2000. [Online]. Available: http://books.google.it/books?id=kv56QgAACAAJ

[17] X.-B. Yin, S. Dong, and E. Wang, Analytical applications of the electrochemiluminescence of tris (2,2-bipyridyl) ruthenium and its derivatives, TrAC Trends in Analytical Chemistry, vol. 23, no. 6, pp. 432 441, 2004. [Online]. Available: http://www.sciencedirect.com/science/article/pii/S016599360400603X

[18] M.-M. Chang, T. Saji, and A. J. Bard, Electrogenerated chemiluminescence. 30. electrochemical oxidation of oxalate ion in the presence of luminescers in acetonitrile solutions, Journal of the American Chemical Society, vol. 99, no. 16, pp. 53995403, 1977. [Online]. Available: http://pubs.acs.org/doi/abs/10.1021/ja00458a028

[19] I. Rubinstein and A. J. Bard, Electrogenerated chemiluminescence. 37. aqueous ecl systems based on tris(2,2bipyridine)ruthenium(2+) and oxalate or organic acids, Journal of the American Chemical Society, vol. 103, no. 3, pp. 512 516, 1981. [Online]. Available: http://pubs.acs.org/doi/abs/10.1021/ja00393a006

[20] W. Miao and J.-P. Choi, Electrogenerated Chemiluminescence. Marcel Dekker,2004.

[21] J. Butler and A. Henglein, Radiation Physics and Chemistry, vol. 15, no. 603, 1980.

[22] T. M. Downey and T. A. Nieman, Chemiluminescence detection using regenerable tris(2,2-bipyridyl)ruthenium(ii) immobilized in nafion,Analytical Chemistry, vol. 64, no. 3, pp. 261268, 1992, pMID: 1554096.[Online]. Available: http://pubs.acs.org/doi/abs/10.1021/ac00027a005

[23] F. Kanoufi and A. J. Bard, Electrogenerated chemiluminescence. 65. an investigation of the oxidation of oxalate by tris(polypyridine) ruthenium complexes and the effect of the electrochemical steps on the emission intensity,The Journal of Physical Chemistry B, vol. 103, no. 47, pp. 10 46910 480, 1999. [Online]. Available: http://pubs.acs.org/doi/abs/10.1021/jp992368s

[24] F. Bolleta, M. Ciano, V. Balzani, and N. Serpone, Polypyridine transition metal complexes as light emission sensitizers in the electrochemical reduction of the persulfate ion, Inorganica Chimica Acta, vol. 62, no. 0, pp. 207 213, 1982. [Online]. Available: http://www.sciencedirect.com/science/article/pii/S0020169300885035

[25] H. S. White and A. J. Bard, Electrogenerated chemiluminescence. 41. electrogenerated chemiluminescence and chemiluminescence of the ru(2,21- bpy)32+-s2o82- system in acetonitrile-water solutions, Journal of the American Chemical Society, vol. 104, no. 25, pp. 68916895, 1982. [Online].Available: http://pubs.acs.org/doi/abs/10.1021/ja00389a001

[26] R. Memming, Mechanism of the electrochemical reduction of persulfates and hydrogen peroxide, Journal of The Electrochemical Society, vol. 116, no. 6, pp. 785790, 1969. [Online]. Available: http://jes.ecsdl.org/content/116/6/785.abstract

[27] A. R. Bowie, M. G. Sanders, and P. J. Worsfold, Analytical applications of liquid phase chemiluminescence reactions a review, Journal of Bioluminescence and Chemiluminescence, vol. 11, no. 2, pp. 6190, 1996. [Online]. Available: http://dx.doi.org/10.1002/(SICI)1099-1271(199603)11:2¡61::AID-BIO406¿3.0.CO;2-O

[28] M. M. Richter, Electrochemiluminescence (ecl), Chemical Reviews, vol. 104, no. 6, pp. 30033036, 2004, pMID: 15186186. [Online]. Available: http://pubs.acs.org/doi/abs/10.1021/cr020373d

[29] J.B. Noffsinger, N.D. Danielson, Analytical Chemistry 59 (1987) 865.

[30] J.K. Leland, M.J. Powell, Journal of the Electrochemical Society 137 (1990) 3127.

[31] G.F. Blackburn, H.P. Shah, J.H. Kenten, J. Leland, R.A. Kamin, J. Link, J. Peterman, M.J. Powell, A. Shah, D.B. Talley, S.K. Tyagi, E. Wilkins, T.J. Wu, R.J. Massey, Clinical Chemistry 37 (1991) 1534.

[32] W.J. Miao, A.J. Bard, Analytical Chemistry 75 (2003) 5825.

[33] W.J. Miao, J.P. Choi, A.J. Bard, Journal of the American Chemical Society 124 (2002) 14478.

[34] C.M. Hindson, G.R. Hanson, P.S. Francis, J.L. Adcock, N.W. Barnett, Chemistry A European Journal 17 (2011) 8018.

[35] Y.B. Zu, A.J. Bard, Analytical Chemistry 72 (2000) 3223.

[36] E.M. Gross, P. Pastore, R.M. Wightman, Journal of Physical Chemistry B 105 (2001) 8732.

[37] S. Workman, M.M. Richter, Analytical Chemistry 72 (2000) 5556.

[38] B. Factor, B. Muegge, S. Workman, E. Bolton, M.M. Richter, Analytical Chemistry 73 (2001) 4621.

[39] D.J. Vinyard, M.M. Richter, Analytical Chemistry 79 (2007) 6404.

[40] J. McCall, C. Alexander, M.M. Richter, Analytical Chemistry 71 (1999) 2523.

[41] J.Z. Kang, X.B. Yin, X.R. Yang, E.K. Wang, Electrophoresis 26 (2005) 1732.

[42] Workman, S.; Richter, M. M. Anal. Chem. 2000, 72, 5556.

[43] Factor, B.; Muegge, B.; Workman, S.; Bolton, E.; Bos, J.; Richter, M. M. Anal. Chem. 2001, 73, 4621.

[44] Leland, J. K.; Powell, M. J. J. Electrochem. Soc. 1990, 137, 3127.

[45] Miao, W.; Choi, J.-P.; Bard, A. J. J. Am. Chem. Soc. 2002, 124, 14478.

[46] Fleet, B.; Kirkbright, G. F.; Pickford, C. J. J. Electroanal. Chem. Interfacial Electrochem. 1971, 30, 115.

[47] Zheng, H.; Zu, Y. J. Phys. Chem. B 2005, 109, 12049.

[48] Honda, K.; Yanaguchi, Y.; Yamanaka, Y.; Yoshimatsu, M.; Fukuda, Y.; Fujishima, A. Electrochim. Acta 2005, 51, 588.

[49] Marselli, B.; Garcia-Gomez, J.; Michaud, P. A.; Rodrigo, M. A.; Comninellis, C. J. Electrochem. Soc. 2003, 150, D79.

[50] Leland, J. K.; Powell, M. J. J. Electrochem. Soc. 1990, 137, 3127.

[51] Pastore, P.; Badocco, D.; Zanon, F. Electrochim. Acta 2006, 51, 5394.

[52] Vinyard, D. J.; Richter, M. M. Anal. Chem. 2007, 79, 6404.

[53] Zu, Y.; Bard, A. J. Anal. Chem. 2000, 72, 3223.

[54] Rubinstein, I.; Bard, A. J. J. Am. Chem. Soc. 1981, 103, 512.

[55] Chang, M.-M.; Saji, T.; Bard, A. J. J. Am. Chem. Soc. 1977, 99, 5399.

[56] Hercules, D. M. Acc. Chem. Res. 1969, 2, 301.

[57] Li, B.; Zhang, Z.; Zheng, X.; Xu, C. Chem. Anal. (Warsaw) 2000, 45, 709.

[58] Bolletta, F.; Ciano, M.; Balzani, V.; Serpone, N. Inorg. Chim. Acta 1982, 62, 207.

[59] White, H. S.; Bard, A. J. J. Am. Chem. Soc. 1982, 104, 6891.

[60] Choi, J.-P.; Bard, A. J. Anal. Chim. Acta 2005, 541, 143.

[61] Hyun J. Kwon* and Ebenezer Akyiano, Department of engineering and computer science, Andrews University.

[62] R. Mark Wightman,Samuel P. Forry,"Rate-Determining Step in the Electrogenerated Chemiluminescence from Tertiary Amines with Tris(2,2-bipyridyl)ruthenium(II)", 2005.

[63] J. Rodriguez-Lopes, "ECL Program (ECL.mph)", 2011.

[64] A. Bard, Electrogenerated Chemiluminescence, ser. Monographs in Electroanalytical Chemistry and Electrochemistry. Taylor & Francis, 2004.

[65] H. N. Choi, S.-H. Cho, and W.-Y. Lee, Electrogenerated chemiluminescence from tris(2,2'-bipyridyl)ruthenium(ii) immobilized in titaniaperfluorosulfonated ionomer composite films, Analytical Chemistry, vol. 75, no. 16, pp. 42504256, 2003, pMID: 14632143.

[66] L. Armelao, R. Bertoncello, S. Gross, D. Badocco, and P. Pastore, Construction and characterization of ru(ii)tris(bipyridine)-based silica thin film electrochemiluminescent sensors. Electroanalysis, vol. 15, no. 9, pp. 803811, 2003.

[67] G. Zhihui and S. Dong, Electrogenerated chemiluminescence from ru(bpy)32+ ion-exchanged in carbon nanotube/perfluorosulfonated ionomer composite films, Analytical Chemistry, vol. 76, no. 10, pp. 26832688, 2004, pMID: 15144175.

[68] W. Gao, X.-H. Xia, J.-J. Xu, and H.-Y. Chen, Three-dimensionally ordered macroporous gold structure as an efficient matrix for solid-state electrochemiluminescence of ru(bpy)32+/tpa system with high sensitivity, The Journal of Physical Chemistry C, vol. 111, no. 33, pp. 12 21312 219, 2007.

[69] H. Wang, G. Xu, and S. Dong, Electrochemiluminescence sensor using tris(2,2'-bipyridyl)ruthenium(ii) immobilized in eastman-aq55dsilica composite thin-films, Analytica Chimica Acta, vol. 480, no. 2, pp. 285 290, 2003.

[70] H. Choi, Y.-K. Lyu, and W.-Y. Lee, Tris(2,2-bipyridyl)ruthenium(ii) electrogenerated chemiluminescence sensor based on sol-gel-derived v2o5/nafion composite films, Electroanalysis, vol. 18, no. 3, pp. 275281, 2006.

[71] L. Dennany, C. F. Hogan, T. E. Keyes, and R. J. Forster, Effect of surface immobilization on the electrochemiluminescence of ruthenium-containing metallopolymers, Analytical Chemistry, vol. 78, no. 5, pp. 14121417, 2006.

[72] J.-K. Lee, S.-H. Lee, M. Kim, H. Kim, D.-H. Kim, and W.-Y. Lee, Organosilicate thin film containing ru(bpy)32+ for an electrogenerated chemiluminescence (ecl) sensor, Chem. Commun., pp. 16021603, 2003.

[73] Electrochemiluminescent detection of hydrogen peroxide with an imaging sensor array, Electrochimica Acta, vol. 49, no. 2223, pp. 3751 3757, 2004.

[74] C. A. Marquette, A. Degiuli, and L. J. Blum, Electrochemiluminescent biosensors array for the concomitant detection of choline, glucose, glutamate, lactate, lysine and urate, Biosensors and Bioelectronics, vol. 19, no. 5, pp. 433 439, 2003.

[75] A. Chovin, P. Garrigue, P. Vinatier, and N. Sojic, Development of an ordered array of optoelectrochemical individually readable sensors with submicrometer dimensions (...), Analytical Chemistry, vol. 76, no. 2, pp. 357364, 2004, pMID: 14719883.

[76] C. Marquette and L. Blum, Self-containing reactant biochips for the electrochemiluminescent determination of glucose, lactate and choline,Sensors and Actuators B: Chemical, vol. 90, no. 13, pp. 112 117, 2003.

[77] W. Zhan, J. Alvarez, and R. M. Crooks, A two-channel microfluidic sensor that uses anodic electrogenerated chemiluminescence as a photonic reporter of cathodic redox reactions, Analytical Chemistry, vol. 75, no. 2, pp. 313318, 2003.

[78] P. Pittet, G.-N. Lu, J.-M. Galvan, R. Ferrigno, K. Stephan, L. J. Blum, and B. Leca-Bouvier, A novel low-cost approach of implementing electrochemiluminescence detection for microfluidic analytical systems,Materials Science and Engineering: C, vol. 28, no. 56, pp. 891 895, 2008.

[79] W. Zhan, J. Alvarez, L. Sun, and R. M. Crooks, A multichannel microfluidic sensor that detects anodic redox reactions indirectly using anodic electrogenerated chemiluminescence,Analytical Chemistry, vol. 75, no. 6, pp. 12331238, 2003.

[80] A. Mamalis, Recent advances in nanotechnology, Journal of Materials Processing Technology, vol. 181, no. 13, pp. 52 58, 2007.

[81] G. Zhihui, S. Yan, W. Mingkui, Z. Feng, and D. Shaojun, Electrochemistry and electrogenerated chemiluminescence of sio2 nanoparticles/(...), Analytical Chemistry, vol. 76, no. 1, pp. 184191, 2004.

[82] Y. Du, B. Qi, X. Yang, and E. , Synthesis of ptnps/aq/ru(bpy)32+ colloid and its application as a sensitive solid-state electrochemiluminescence sensor material, The Journal of Physical Chemistry B, vol. 110, no. 43, pp. 21 66221 666, 2006.

[83] Z. Chang, J. Zhou, K. Zhao, N. Zhu, P. He, and Y. Fang, Ru(bpy)32+-doped silica nanoparticle dna probe for the electrogenerated chemiluminescence detection of dna hybridization, Electrochimica Acta, vol. 52, no. 2, pp. 575 580, 2006.

[84] Z. Ding, B. M. Quinn, S. K. Haram, L. E. Pell, B. A. Korgel, and A. J. Bard, Electrochemistry and electrogenerated chemiluminescence from silicon nanocrystal quantum dots, Science, vol. 296, no. 5571, pp. 12931297, 2002.

[85] L. Dennany, R. J. Forster, and J. F. Rusling, Simultaneous direct electrochemiluminescence and catalytic voltammetry detection of dna in ultrathin films, Journal of the American Chemical Society, vol. 125, no. 17, pp. 52135218, 2003.

[86] J. Li, Y. Xu, H. Wei, T. Huo, and E. Wang, Electrochemiluminescence sensor based on partial sulfonation of polystyrene with carbon nanotubes,Analytical Chemistry, vol. 79, no. 14, pp. 54395443, 2007.

[87] H. Wei, Y. Du, J. Kang, and E. Wang, Label free electrochemiluminescence protocol for sensitive dna detection with a tris(2,2'-bipyridyl)ruthenium(ii) modified electrode based on nucleic acid oxidation, Electrochemistry Communications, vol. 9, no. 7, pp. 1474 1479, 2007.

[88] Y. Tao, Z.-J. Lin, X.-M. Chen, X. Chen, and X.-R. Wang, Tris(2,2-bipyridyl)ruthenium(ii) electrochemiluminescence sensor based on carbon nanotube/organically modified silicate films, Analytica Chimica Acta, vol. 594, no. 2, pp. 169 174, 2007.

[89] H. N. Choi, S.-H. Cho, Y.-J. Park, D. W. Lee, and W.-Y. Lee, Solgel-immobilized tris(2,2-bipyridyl)ruthenium(ii) electrogenerated chemiluminescence sensor for high-performance liquid chromatography, Analytica Chimica Acta, vol. 541, no. 12, pp. 47 54, 2005.

[90] X. Hun and Z. Zhang, Electrogenerated chemiluminescence sensor for itopride with ru(bpy)32+-doped silica nanoparticles/chitosan composite films modified electrode, Sensors and Actuators B: Chemical, vol. 131, no. 2, pp. 403 410, 2008.

[91] P. Pastore, D. Badocco, and F. Zanon, Influence of nature, concentration and ph of buffer acidbase system on rate determining step of the electrochemiluminescence of ru(bpy)32+ with tertiary aliphatic amines, Electrochimica Acta, vol. 51, no. 25, pp. 5394 5401, 2006.

[92] L. Zhang and X. Zheng, A novel electrogenerated chemiluminescence sensor for pyrogallol with core-shell luminol-doped silica nanoparticles modified electrode by the self-assembled technique, Analytica Chimica Acta, vol. 570, no. 2, pp. 207 213, 2006.

[93] L. Luo and Z. Zhang, Sensors based on galvanic cell generated electrochemiluminescence and its application, Analytica Chimica Acta, vol. 580, no. 1, pp. 14 17, 2006.

[94] T. Kuwabara, T. Noda, H. Ohtake, T. Ohtake, S. Toyama, and Y. Ikariyama, Classification of dna-binding mode of antitumor and antiviral agents by the electrochemiluminescence of ruthenium complex, Analytical Biochemistry, vol. 314, no. 1, pp. 30 37, 2003.

[95] W. Miao and A. J. Bard, Electrogenerated chemiluminescence. 72. determination of immobilized dna and c-reactive protein on au(111) electrodes using tris(2,2'-bipyridyl)ruthenium(ii) labels, Analytical Chemistry, vol. 75, no. 21, pp. 58255834, 2003, pMID: 14588023.

[96] Y. Li, H. Qi, Y. Peng, J. Yang, and C. Zhang, Electrogenerated chemiluminescence aptamer-based biosensor for the determination of cocaine, Electrochemistry Communications, vol. 9, no. 10, pp. 2571 2575, 2007.

[97] M.-L. Calvo-Muoz, A. Dupont-Filliard, M. Billon, S. Guillerez, G. Bidan, C. Marquette, and L. Blum, Detection of dna hybridization by abei electrochemiluminescence in dna-chip compatible assembly, Bioelectrochemistry, vol. 66, no. 12, pp. 139 143, 2005.

[98] W. Miao and A. J. Bard, Electrogenerated chemiluminescence. 77. dna hybridization detection at high amplification with [ru(bpy)3]2+-containing microspheres. Analytical Chemistry, vol. 76, no. 18, pp. 53795386, 2004, pMID: 15362895.

[99] Electrogenerated chemiluminescence. 80. c-reactive protein determination at high amplification with [ru(bpy)3]2+-containing microspheres, Analytical Chemistry, vol. 76, no. 23, pp. 71097113, 2004, pMID: 15571366.

[100] W. Zhan and A. J. Bard, Electrogenerated chemiluminescence. 83. immunoassay of human c-reactive protein by using ru(bpy)32+-encapsulated liposomes as labels, Analytical Chemistry, vol. 79, no. 2, pp. 459463, 2007.

[101] X. Liu, L. Shi, W. Niu, H. Li, and G. Xu, Environmentally friendly and highly sensitive ruthenium(ii) tris(2,2-bipyridyl) electrochemiluminescent system using 2-(dibutylamino)ethanol as co-reactant, Angewandte Chemie International Edition, vol. 46, no. 3, pp. 421424, 2007.

[102] X.Q. Liu, L.H. Shi, W.X. Niu, H.J. Li, G.B. Xu, Angewandte Chemie International Edition 46 (2007) 421.